NUMERICAL SIMULATION OF WATER WAVE GENERATION

by

Liting Zhang

A Thesis

Submitted to the Faculty of Purdue University

In Partial Fulfillment of the Requirements for the degree of

Master of Science in Mechanical Engineering

Department of Electrical and Computer Engineering

Hammond, Indiana

August 2021

THE PURDUE UNIVERSITY GRADUATE SCHOOL

STATEMENT OF COMMITTEE APPROVAL

Dr. Xiuling Wang, Chair

Department of Mechanical and Civil Engineering

Dr. Harvey Abramowitz

Department of Mechanical and Civil Engineering

Dr. Ran Zhou

Department of Mechanical and Civil Engineering

Approved by:

Dr. Chenn Zhou

ACKNOWLEDGMENTS

I would like to express my deepest appreciation first to my thesis advisor, Dr. Xiuling Wang, for her constant and enthusiastic encouragement and useful guidance. She had been providing me with a lot of precious research skills, valuable and constructive advice for my thesis as well. She is always patient to help me overcome the obstacles and challenges during the preparation and development of this research work. Her willingness to offer so much of her time has been greatly appreciated.

Secondly, I would like to extend my sincere thanks to all the staff and faculty in the department of Mechanical and Civil Engineering in Purdue Northwest. They are always ready to answer a variety of inquiries and support me in staying on track. I am grateful for Dr. Ran Zhou, and Dr. Harvey Abramowitz who are willing to be the members of examining committee.

Finally, my thanks would go to my beloved family and friends who stand by me with their understanding, support, and love. They are always profound belief in my work and in my abilities which plays a decisive role in my study.

TABLE OF CONTENTS

LIST OF TABLES

LIST OF FIGURES

NOMENCLATURE

A	amplitude, m
d	water depth, m
g	gravity acceleration, m/s^2
h	depth, m
H	wave height, m
k	wave number, m^{-1}
k	normal unit vector
L	wavelength, m
m	coordinate normal to the bottom
N	the unit exterior normal vector
p	phase
q	phase
S	the transposition of the piston, m
S_0	the maximum displacement of the wave generator, m
t	time, s
T	wave period, s
u	the velocity component in x direction, m/s
v	wave velocity, m/s
V	vector velocity, m/s
w	the velocity component in z direction, m/s
z	the position change from the free water surface to the sea floor, m
Z	vertical direction
η	elevation of the wave, m
φ	potential function
φ_1	first-order term for stokes second order theory
φ_2	the second term for stokes second order theory
ω	the wave frequency, Hz
α_q	the volume fraction of the q^{th} fluid in the cell

$\dot{m}_{pq}$ the mass transfer from the q^{th} phase to the p^{th} phase

$\dot{m}_{qp}$ the mass transfer from the p^{th} phase to the q^{th} phase

ABSTRACT

At present, caused by a large amount of wave energy resources and huge energy capacity, the development and utilization of wave energy have come to be an essential development focus of wave energy manufacturing. The purpose of this research is to simulate the ocean in an offshore environment. A three-dimensional computational fluid dynamics (CFD) model was used to analyze the propagation of ocean waves. The Volume of Fluid (VOF) multiphase model and laminar model were used to analyze wave propagation in offshore conditions. Function Methodology and Mobile Methodology were implemented by applying User Defined Function (UDF) code which characterizes transient velocity profile. The parametric study was performed to analyze how velocity and amplitude change. The models were first validated by comparing them with previous analytical wave solutions. To prevent the reflection of the wave, a damping term was added by using User Define Function to define the viscosity of the water phase.

1. INTRODUCTION

1.1 Background and Motivation

The data of U.S. energy supply, which is come from the Energy Information Administration is shown in Figure 1 [1]. As indicated in Figure 1, barely a little portion of the energy supply comes from wind turbines and any other renewable resources, which was 12% in 2020, while there are 80% of the energy supply comes from the fossil fuels. Nuclear energy only provides 9% of the energy supply.

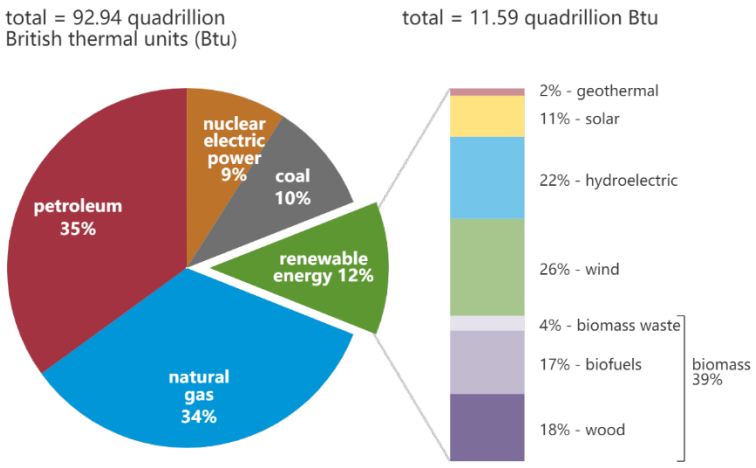

Figure 1. U.S. Primary energy consumption, 2020.

While the importance of renewable energy technologies is recognized, it is critical to realize that fossil fuels remain the primary source of energy we collect. Moreover, according to the Energy Information Administration, this situation will continue to exist in the coming decades. This illustrates the special challenges we face as we move away from fossil fuels.

After years of fossil fuel use, the power available to a given society has been limited, and a wide range of innovative possibilities are waiting to be considered. The historic Paris Climate Agreement of 2016 sent a clear signal that the global shift to low carbon energy is critical and will continue to shift to clean energy.

More recently, because of the topic of climate change, there is again a growing concern worldwide for renewable energy, including wave energy. The oceans contain immense amounts of energy dispersed along the world's seashore.

Ocean simulation technology is widely used in virtual reality and other fields. Describing ocean waves involves a high degree of difficulty, not only because wavelengths vary from millimeters to kilometers, but also because wave movement is associated with wind, tides, and topography. Although the current ocean simulation technology is extremely realistic, finding a straightforward and efficient way to simulate ocean waves remains a challenge.

1.2 Literature Review

With the development of computational fluid dynamics software, preliminary studies can now be conducted cheaply and quickly. This means that the numerical model used can be representative of the real environment. Finite element method, finite difference method, and boundary volume method are used in the numerical model. At the input boundary, waves are created and decay near the output boundary.

A lot of contributions and improvements on ocean wave simulation have been achieved. Numerical piston wave generator is used to generate the desired wave in the most study. To simulate three-dimensional fully nonlinear numerical waves, Kim et al (2004) used a numerical wavemaker by specifying the water particle velocities at the boundary of the wave generator [2]. A directional incident wave from the inflow boundary was produced by the serpentine motion along the direction of the wave generator. Within a synthetically damped region at the end of the tank, the outgoing wave was statistically dissipated. Wang et al (2006) also use a wave generator of the piston kind to integrate into the computational field in order to generate the required incident wave [3]. Based on Navier-Stokes equations, the completely nonlinear free surface boundary conditions of three-dimensional numerical viscous wave tank were created. To discretize subjective variance equation, the finite analytical technique was used. Make use of this model, the generation and transmission of waves were analyzed.

Different numerical methodologies for generation waves are compared. Zabihi et al (2015) offered the ability of two different arithmetic software to produce the regular gravity waves in a wave tank [4]. According to Navier-Stokes and VOF equations, the wave was generated by Fluent and Flow-3D software. The height of the free surface and the horizontal component of the wave

velocity are two parameters to be considered. The results show that, in some cases, Flux3D can catch the height of the free surface more precisely. Wave energy dissipation and wave reflection are critical parts of numerical models. By assessing four different slopes, the minimum slope required for wave energy dissipation was concluded. To study the regular gravity waves, two distinct numerical techniques were used by Gomes et al (2009) [5]. Fluent was used to statistically simulate the wave generation, and multiphase fluid volume (VOF) model was used to reconstruct the wave propagation in the wave tank.

Open-source technique from CFD model is broadly applied to generate the wave. To simulate the wave transmission underwater, Kamath et al (2015) used the open source CFD model [6]. When the wave propagates at the top of the rod, changes in the wave that produce higher-order harmonics in the wave tank can be detected. The difference of wave conversion process under two different type of incident wave heights is studied. The shoal phenomenon occurred more easily at high incident wave heights than at low incident wave heights. To provide comprehensive evaluation indexes and methods for the generation of the wave and concentration under monochrome and polychrome sea conditions, Windt et al (2019) used the main numerical wave generator provided by Open Foam Open Source CFD software [7]. An implementation of a pulse-source wave generator in which the pulse-source function can be self-calibrated to generate a desired wave sequence in deep water or shallow water at a specified moment in time and space point. By using the open-source hydrodynamic framework REEF3D, Wang et al (2020) studied the three main phase analytic wave models, explained the advancement and numerical completion of REEF3D, and demonstrated the numerical assimilation and differences between wave models [8]. These baseline studies providing insights into the computational performance of each wave simulation technique and its limitations on the hydrodynamic phenomena of different wave types. The variety of test cases improves to choose a trained wave model for different situations.

Besides study gravity wave, pressure wave also has research value. Yang et al (2017) established a basic CFD model with a pressure wave generator which is used to connect upstream and downstream pipes, the pressure waves generated in the water hammer principle were analyzed [9]. The generation procedure of pressure wave in pipeline flow was analyzed, and the frequency and amplitude physical characteristics of pressure wave were acquired.

Since there are a lot of methodology to simulate the wave propagation. Li et al (2019) compared the Spectral Wave Explicit Navier Stokes Equations method, Internal Wave Generator

method, and the Relaxation Zone method, which were the wave modeling methods of three two-phase CFD solvers [10]. The first two methods generated and attracted waves within a specific area, however, the third reached a prospective viscous coupling in the whole domain. A group existing wave exit methods which were frequently used in free surface simulations were compared by Choi et al (2020) [11]. Extending the mesh, linear damping sources, rising viscosity, and reduction schemes were included in these methodologies. The comparison between the propagation of the regular incident wave and the lessening of radioactivity wave was conducted.

It is important to explore the fluid flow close to an interface malformed by generating waves by studying the development of the fluid flow governing equations. The governing equations of fluid flow, involving momentum, preservation of mass, and energy balance were derived by Yousefi et al (2020) [12]. To obtain the mean component, wave-induced component, and turbulent component, all the equations were further decomposed. In addition, by considering the commotion of wavelength was greater than the amplitude of the wave, the governing equations of motion were further streamlined. In the orthogonal curvilinear coordinates, the boundary layer equation was expressed as the corresponding decomposition equation of the mean-field, wavefield, and turbulence field by using the quasilinear analysis method. Finally, the vorticity equation was derived in the orthogonal curvilinear coordinate system, and the corresponding velocity-vorticity formula was obtained.

The effect of ocean conditions on the air-sea momentum flow of wind stress is a poorly understood aspect of wind-wave interaction, especially during gales. To replicate research laboratory studies of phase-mean flow over waves under strong forcing conditions, Husain et al (2019) used a sinusoidal train upwind large eddy simulation (LES) [13]. Both LES and interpretations used a wave-tracking coordinate system to decay wind speed into average, wave consistency, and turbulent variability elements. The LES results of mean wind profile, wave, and turbulent stress components are in good accord with the findings of the observations. Both LES and observations show an increase in turbulent stress and mean wind shear at the peak, indicating the effect of intermittent airflow separation events. Near the peak, the nonlinearity and instability of the experimental wave would affect the separation and shading of the airflow. How do finite-amplitude wave characteristics control aerodynamics, which may greatly affect the mean wind profile, equivalent surface roughness, as well as the drag coefficient, was illustrated by these results.

Evidently, numerous researches have focused on the wave generation using numerical model. There are a variety of field research, wave experiments, and computational simulation that are applied to investigate wave force. However, few research has ever combined comprehensive effects to analyze the wave effect. The case study presented in this thesis is a numerical and graphical analysis of wave generation processes with different characteristics. Furthermore, detail study about avoiding wave reflection was carried.

2. MATERIAL AND METHODS

2.1 Water Wave

Standing on the beach and watching the waves roll and break, one might think that the water is moving toward the shore. But in fact, there is no water accumulating on the beach. Watching a piece of debris float out of the broken wave, it can be seen to move ashore on the crest of the wave and then return at the same distance as the trough. The debris moves along a roughly circular path perpendicular to the water surface. Water waves are usually defined as surface waves, which are a mixture of compressional and transverse waves. In oceanography, surface waves are the deformation of the sea surface. The deformation propagates at the speed of a wave, while the water molecules stay in the same position on average. However, this energy moves toward the coast. Most waves are generated by wind, and the energy generated from the wind offshore is carried to shore by the waves.

The energy of a wave depends on its wave height, wavelength, and the distance at which it breaks. When a wave with a larger amplitude falls back to sea level, it releases more energy than a wave with a smaller amplitude at the same wavelength. The energy per square meter is proportional to the square of the height. McCormick (1976) summarized the characteristic and velocity profile for different water wave [14].

2.1.1 Deep water wave

Deep water waves in the ocean are waves created by the wind. They can be generated by local winds or distant winds. When the water beneath a wave is deeper than half of its wavelength ($d > \frac{1}{2}L$, where d refers to the water depth, and L refers to wavelength), these waves are called deep water waves. Most open waves are considered as the deep-water waves. As the result of the water is deeper than the wave base, deep water waves are not disturbed by the ocean floor, so their speed depends only on the wave period:

$$v = \frac{gT}{2\pi} \tag{1}$$

where g refers to the gravity acceleration.

Water molecules in deep water waves move in the circular orbits, which can be shown in Figure 2. The diameter of the orbit decreases with distance from the water surface. The motion is felt at a distance of about one wavelength, at which the energy of the wave is negligible.

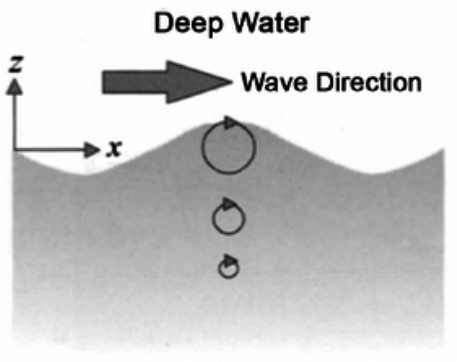

Figure 2. The orbital motion in deep water.

2.1.2 Intermitted water wave

Intermediate waves are found in depths between $1/2$ and $1/20$ of the wavelength ($\frac{1}{20}L < d < \frac{1}{2}L$). The behavior of intermediate water wave is much more complex, which is because that their speed is influenced by wave period, wavelength, and depth. The speed of an intermediate wave is calculated as:

$$v = \frac{gT}{2\pi} \tan\left(2\pi \frac{d}{L}\right) \tag{2}$$

The motion of the circle decreases with increasing depth because waves have less effect on deeper waters and the diameter of the circle decreases, which can be seen in Figure 3. Eventually at a certain depth there is no more circular motion, and the water is unaffected by surface waves. This depth is the wave base, equal to half the wavelength. Since most ocean waves have wavelengths less than a few hundred meters, most of the deep ocean is unaffected by surface waves, so even during the strongest storms, Marine life or submarines can dive into the wave base to avoid the waves.

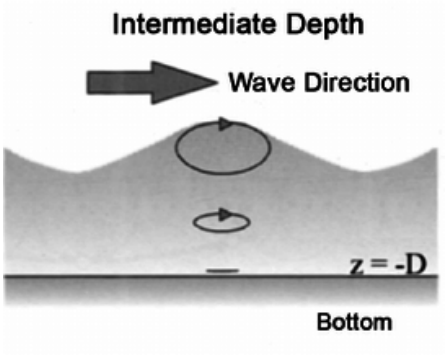

Figure 3. The orbital motion in intermitted water.

2.1.3 Shallow water wave

Shallow water waves will occur when the depth is less than $1/20$ of the wavelength ($d < \frac{1}{20}L$). In other words, the wave is called the "touch bottom" because the depth is shallower than the wave base, which leads to the result that the orbital motion is affected by the ocean floor. Due to the shallower depth, the track flattens out, and eventually, the motion of the water becomes horizontal, rather than circular just above the bottom. The speed of shallow-water waves is independent of their wavelength, it depends only on the depth:

$$v = \sqrt{gd} \tag{3}$$

Figure 4 shows that the orbits of the molecules of shallow-water waves are more elliptical.

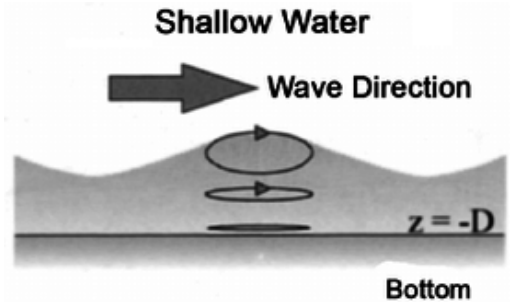

Figure 4. The orbital motion in shallow water.

2.2 Gravity Wave

Gravity waves in hydromechanics are waves that occur in a liquid medium or between two media (such as the atmosphere and the ocean) and have a restorative force due to gravity or

buoyancy. When a small mass of liquid leaves the surface (interface type) or moves into a region of liquid density (inside type), the mass of liquid swings from an equilibrium state to an equilibrium state in a wave by gravity. The type inside a liquid medium is called an internal wave, and the type between two interfaces is called surface gravity wave or surface wave. It usually propagates along the surface and decays in a direction perpendicular to the surface (a so-called nonuniform wave). The depth of penetration into the surface does not exceed one wavelength, and since this depth depends on the wavelength, the dispersion of the wave results. However, when the depth of the fluid h is much smaller than the wavelength of the long wave limit, the wave pressure is approximately uniform across the whole section, the wave is non-dispersive.

A good example for gravity wave is the ocean wave, that's the reason choose the gravity wave to study the ocean wave. Gravity waves are considered as the regular waves and are constant over each time period. In this thesis, two theories of gravity waves are deliberated: one was linear wave theory, which is suitable for long waves of small amplitude, the other one was stokes second order nonlinear wave theory which is appropriate for long waves of large amplitude.

Gravity waves must satisfy the following three boundary conditions: free surface kinematic condition, free surface dynamic condition and bottom condition.

2.2.1 Free surface kinematic condition

Water particles cannot traverse the free surface due to the free surface kinematic condition. To alleviate the problem of particle velocity, where $Z = \eta$, should be equal to the normal speed at the free surface. The arithmetic condition is:

$$V|_{Z=\eta} \approx \frac{\partial \eta}{\partial t} k = \frac{\partial \varphi}{\partial Z}|_{Z=0} k \tag{4}$$

where φ refers to a potential function and k refers to the normal unit vector.

2.2.2 Free surface dynamic condition

The pressure on the free surface is equal to zero at any point x and at any time t in the free surface dynamic condition. Mostly, Bernoulli equation is applied to the free surface to obtain:

$$\frac{\partial \varphi}{\partial t} + g\eta + \frac{1}{2}V^2 = 0 \tag{5}$$

where φ refers to a potential function, g refers to gravity, η refers to the elevation of free surface and V refers to the velocity. Through using this condition of dynamic linearization, the second boundary condition is able to be linearized:

$$\eta = -\frac{1}{g}\frac{\partial \varphi}{\partial t}|_{Z=\eta} \tag{6}$$

2.2.3 Bottom condition

Bottom condition denotes that the bottom is horizontally impermeable. Arithmetically, in where $Z = -h$:

$$\frac{\partial \varphi}{\partial Z} = 0 \tag{7}$$

The continuity equation holds when dealing with a continuous fluid in a wave. If the flow is irrotational, the velocity may be represented as a potential function, then the continuity equation is:

$$\nabla^2 \varphi = 0 \tag{8}$$

The velocity potential is a solution to Equation 8 that meets the boundary conditions:

$$\varphi = \frac{ag}{\omega}\frac{cosh(kz + kh)}{cosh(kh)}sin(kx - \omega t) \tag{9}$$

According to Equation 9, the following velocity components can be defined as:

$$u = \frac{\partial \varphi}{\partial x} = \frac{agk}{\omega}\frac{cosh(kz + kh)}{cosh(kh)}cos(kx - \omega t) \tag{10}$$

$$w = \frac{\partial \varphi}{\partial z} = \frac{agk}{\omega} \frac{sinh(kz + kh)}{cosh(kh)} sin(kx - \omega t) \quad (11)$$

where u refers to the velocity component in x direction and w refers to the velocity component in z direction.

The free surface motion can also be highlighted as following equation:

$$\eta = A\, cos(kx - \omega t) \quad (12)$$

The other theory discussed above is Stokes theory, which holds that wave motion characteristics, such as velocity potential, may be described by a sequence of tiny disturbances. In deeper seas, this also applies to larger wave heights. The velocity potential, according to this idea, is:

$$\varphi = \varepsilon\varphi_1 + \varepsilon^2\varphi_2 + \varepsilon^3\varphi_3 + \cdots \quad (13)$$

The solution contains the linear theory represented by the first-order term φ_1. Expand to the second term φ_2 stands for stokes second order theory and so on.

2.3 Linear wave theory

Linear is a mathematical term. A relationship in which the dependent variable is proportional to the independent variable is called a linear relationship; Otherwise, it's a non-linear relationship. If the physical quantity (or its perturbation) in the wave is small enough that the quadratic term and the term above the quadratic term in the equation of motion are negligible compared with the first order term, then it is the first order term that determines the wave's properties and behavior. Such waves are called linear in the sense of linear. The theory implies a uniform mean depth for the fluid layer and that the fluid flow is inviscid, incompressible, and irrotational. This linear theory is frequently applied to provide a rapid and approximate approximation of wave properties and impacts. This estimate is correct for both shallow and deep ocean waves. To describe the motion of gravity waves on a fluid surface, linear wave theory employs a velocity potential method.

According to McCormick (1976), due to the natural inclination of fluids is to remain in balance, waves exist on the free surface [14]. When an object is thrown into a reservoir, a

commotion will be formed which means a surface wave is formed. The subsequent movement of the water surface is the result of gravity and tends to allow the water to return undisturbed to its place. These waves are known as gravity waves because they are generated by gravity. Dean and Dalrymple (1991) believed that an additional factor that could affect free water disturbance was the influence of wind [15]. In addition, depending on the force acting on the water, waves may come in a variety of sizes and forms. In Figure 5, the main characteristics of the wave can be observed.

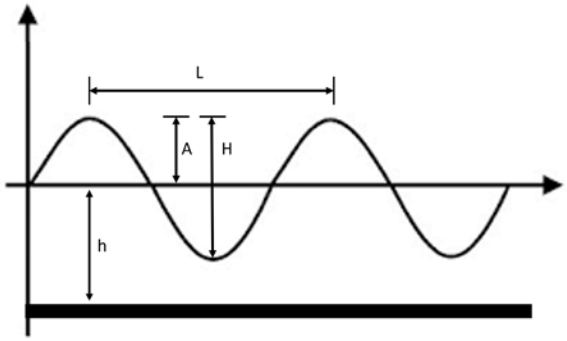

Figure 5. Characteristics of wave.

Corresponding to Figure 5, the distance from the sea floor to the mean height of sea level is denoted by h, A refers to the amplitude, H represents the height, which is the distance between crest and trough, and L refers to the wavelength, which can be determined by:

$$L = \frac{gT^2}{2\pi} tan\, h\left(\frac{2\pi h}{L}\right) \tag{14}$$

where g denotes gravity acceleration and T denotes wave period, which may be defined as the amount of time it takes for a wave to complete a cycle, in this case it is the time needed to propagation a distance of a wavelength. All waves, whether gravitational, acoustic, or electromagnetic, follow a wave equation.

2.4 Nonlinear Wave Theory

Wave action is often the main cause of coastal engineering, Marine engineering, etc. All real waves are nonlinear waves, and there is a large error in the study of small amplitude wave

theory, which is linear wave theory, as a result, it is necessary to use nonlinear finite-amplitude waves to solve practical wave problems. According to the finite-amplitude wave theory, there are three main types of waves: Stokes wave, elliptic cosine wave, and solitary wave.

Surface gravity waves require boundary conditions to be imposed at the free surface position. In 1847, Stokes introduced in 1847 a way for expressing the velocity potential function of a wave, expand it to match the nonlinear boundary condition. Stokes wave is not suitable for shallow water wave. Elliptic cosine wave can be applied to shallow water wave, The waveform remains unchanged during the propagation process, when the wavelength tends to infinity, it is a solitary wave.

2.5 Function Methodology

Stokes second order theory is a famous variant of the linear theory that contains an extra high order component in the creation. According to Horko (2007), the motion equation of free-form surface in Stokes second order theory can be determined [16]:

$$\eta = Acos(kx - \omega t) + \ ... \\ ... + \frac{A^2 k\, cosh(kh)}{4sinh^3(kh)}[2 + cosh(2kh)]\, cos\, 2(kx - \omega t) \tag{15}$$

Furthermore, the velocity components are:

$$u = \mathrm{A}gk\frac{cosh\, kz}{\omega\, cosh\, kh} cos(kx - \omega t) + ... \\ ... + A^2 \omega k \frac{cosh\, 2kz}{sin^4(kh)} cos\, 2(kx - \omega t) \tag{16}$$

$$w = Agk\frac{sinh\, kz}{\omega\, sinh\, kh} sin(kx - \omega t) + ... \\ ... + A^2 \omega k \frac{sinh\, 2kz}{cos^4(kh)} sin\, 2(kx - \omega t) \tag{17}$$

where k refers to the wave number which is provided by $k = 2\pi/L$, and L refers to the wavelength, z refers to the position change from the free water surface to the sea floor, ω refers to the wave frequency, which is defined by $\omega = 2\pi/T$.

Function methodology involves applying the inlet velocity to the wave generator by using a User Defined Function (UDF), and the velocity differs regarding to Equation 16 and Equation 17, which is suitable for a wave generator with velocity deviation based on the Stokes second order theory proposed by Horko (2007) [16].

2.6 Mobile Methodology

By utilizing the boundary conditions of the moving wall surface to a wave generator, which is similar to piston motion, there is Mobile Methodology. To allow velocity variations to be applied to moving walls through User-Defined Functions (UDFs), dynamic mesh technology was used. Based on the characteristics of the wave to be generated, it is possible to control the motion of the piston. Additionally, the period, and height of the wave must be known. The required characteristics of the wave displacement carried by the piston can be obtained by using the transfer function, which links the wave height and piston displacement, in order to create the wave with the required properties. Dean and Dalrymple (1991) defined the transfer function [15]:

$$\frac{H}{S} = \frac{2(\cosh(2kh) - 1)}{\sinh(2kh) + 2kh} \tag{18}$$

where H refers to the wave height, S refers to the transposition of the piston, h refers to the water depth and k refers to the wave number which is provided by $k = 2\pi/L$, where L refers to the wavelength.

Delineated by Liu et al, (2008) the motion equation is [17]:

$$x(t) = \frac{S_0}{2}\left(1 - e^{-\frac{5t}{2T}}\right)\sin(\omega t) \tag{19}$$

where S_0 refers to the wave generator's greatest displacement, T refers to the wave period and ω refers to the wave frequency, which is defined by $\omega = 2\pi/T$.

The wave generator velocity is given by:

$$v(t) = \left(\frac{S_0}{2}\right)\left[\left(1 - e^{-\frac{5t}{2T}}\right)\omega\, cos(\omega t) + \frac{5}{2T}e^{-\frac{5t}{2T}} sin(\omega t)\right] \tag{20}$$

Figure 6 shows the schematic of the wave tank. Equation 19 and Equation 20 are applied to the wave maker to generate the wave.

Figure 6. Schematic of wave tank.

2.7 VOF Model

A surface tracking approach based on a fixed Euler grid is the VOF model. VOF model is mostly used to calculate a time-dependent solution [18]. The VOF model may simulate two or more immiscible fluids based on the fact that two or more fluids (or phases) do not mix. A set of momentum equations is shared by all fluid components. The phase interface of each computation unit may be traced by introducing the phase volume fraction variable. The movement of big bubbles in a liquid phase, the flow of a liquid following a dam collapse, and the stability or transient tracking of any liquid-gas interface are examples of typical VOF model uses.

The total of the volume fractions of all phases in each control volume equals one unit. As long as the volume fraction for each stage is known at each location, the fields for all variables and characteristics are shared by the stages and reflect the volume average. As a result, based on volume fraction values, variables and characteristics in each particular cell reflect pure or mixed phases. To put it another way, if the volume fraction of the q^{th} fluid in the cell is denoised as α_q, there are three conditions might occur:

$\alpha_q = 0$: The cell is empty (of the q^{th} fluid).

$\alpha_q = 1$: The cell is full (of the q^{th} fluid).

$0 < \alpha_q < 1$: The cell contains the interface between the q^{th} fluid and one or more other fluids.

Assign appropriate attributes and variables to each control body in the domain based on the local value of α_q.

Solving the continuity equation for one or more phase volume fractions, the interface between two phases can be tracked. For the q^{th} phase, the continuity equation:

$$\frac{1}{\rho_q}\left[\frac{\partial}{\partial t}(\alpha_q \rho_q) + \nabla \cdot (\alpha_q \rho_q \overrightarrow{v_q})\right] = S_{\alpha_q} + \sum_{p=1}^{n}(\dot{m_{pq}} - \dot{m_{qp}}) \quad (21)$$

where $\dot{m_{pq}}$ refers to the mass transfer from the q^{th} phase to the p^{th} phase. By contrast, $\dot{m_{qp}}$ refers to the one from the p^{th} phase to the q^{th} phase. S_{α_q} is considered to be zero by default, however, it can be identified a continual or user-defined quality source for each phase.

A momentum equation across the full domain and the associated velocity field can be solved by sharing among the phases. The momentum equation can be defined as follows, depending on the volume fraction of all the phases by characteristics ρ and μ:

$$\frac{\partial}{\partial t}(p\vec{v}) + \nabla \cdot (p\vec{v}\vec{v}) = -\nabla_p + \nabla \cdot [\mu(\nabla\vec{v} + \nabla\vec{v}^T)] + \rho\vec{g} + \vec{F} \quad (22)$$

One of the limitations of the shared field calculation is that the precision of the velocities calculated in the vicinity of the interface may be negatively influenced when there is a huge velocity difference between the two phases.

2.8 Numerical Settings

Pressure-based solver was used under transient condition. Based on the volume fluid (VOF) method, the numerical model is used, which allows a wave trough to be computed and simulated in a very realistic manner by studying the interaction between water phase and air phase. In Mobile Methodology, dynamic mesh is used, according to Fluent Tutorial [20].

Table 1. Boundary Conditions.

Name	Boundary	Description
Inlet	Velocity inlet	User Define Function
Outlet	Pressure outlet	Normal to Boundary
Side	Wall	Stationary Wall, No Slip
Gravity	Gravitational Acceleration	Z=-9.81 m/s^2
Models	Volume of Fluid	Implicit Body Force

3. RESULTS AND DISCUSSION

3.1 Computational Domain

To make sure simulation results reasonable, the computational model for wave effects in this thesis was first validated with a numerical result conducted by Gomes et al. The computational domain of water tank was consistent with the numerical study by Gomes and has the same dimensions. The x-axis was extended along with the wave direction. The computational domain has one velocity inlet, the boundary conditions depend on one of two methods chosen. A pressure outlet is set at the top of the wave trough and the atmospheric pressure boundary condition is adopted. Under the wall boundary condition, the velocity is zero. The fluid domain was 6 m long, 0.6 m wide, and 0.8 m high. The computational domain is shown in Figure 7. The original point for z is from the bottom of the tank. The depth of wave tank, which is the distance between the seafloor and mean sea level, was set to be 0.5m high. In other words, the top of the wave tank which was from 0.5m high to 0.8m high was air region.

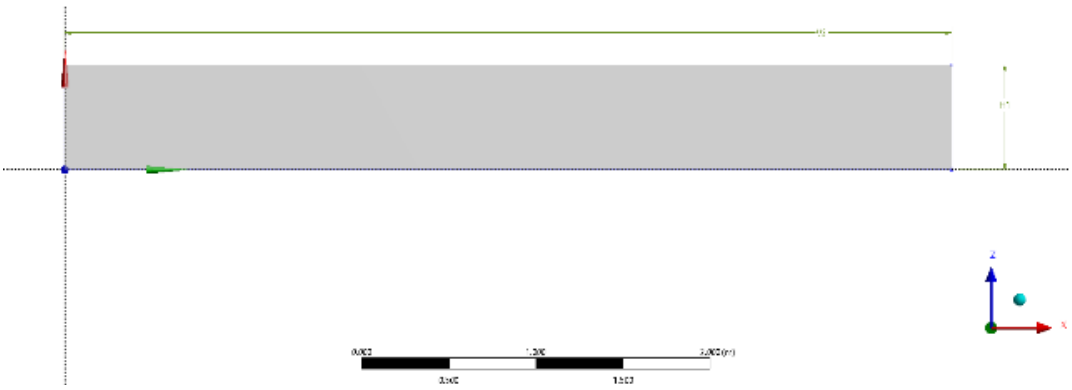

(a) Front view

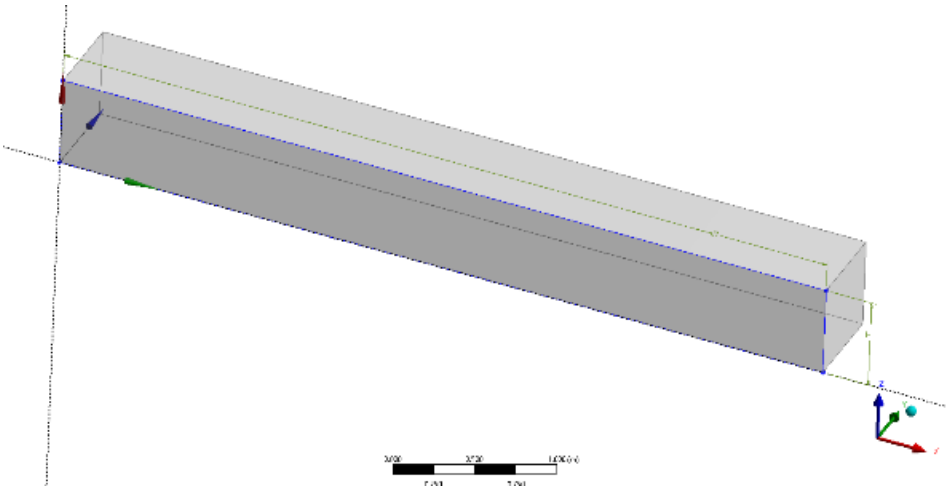

(b) Overall view

Figure 7. Computational domain for wave tank.

Figure 8 shown the computational mesh used which is the medium mesh corresponding to the mesh independence study in the nest section, since the medium mesh give the reasonable result and possibility of wave generation. There were 360, 000 hexahedral cells and 382, 571 nodes.

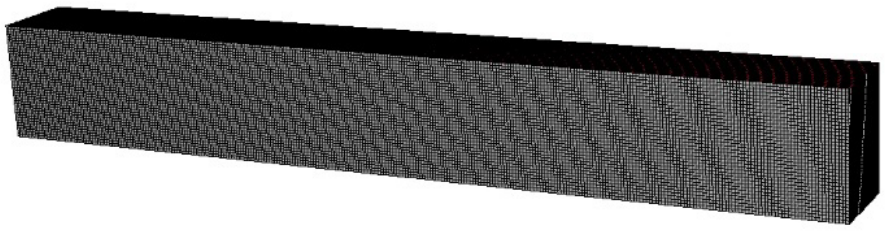

Figure 8. Computational mesh of wave tank.

3.2 Simulations on Mesh Independence Study

In general, the finer the mesh, the more accurately the outline of the geometry can be captured, and the more "data points" on the geometry, the more accurate displacement and stress responses can be generated. The analyst can perform grid independence studies to determine how dependent the results are on grid density. Simply put, run several simulations to make sure our results are mesh independent. Mesh independence research is critical in CFD due to the nature of CFD simulations and the underlying mathematics. In CFD, meshing can and does affects the final solution. In mechanics, this type of analysis can improve the reliability of the results or reduce the calculation time.

To examine how the mesh fineness would affect the simulation result, mesh independence study is carried out by using Function Methodology added the damping term to avoid the wave reflection. For convention, FM refers to Function Methodology, and MM refers to Mobile Methodology. Table 2 shows the numerical simulations performed for mesh independence study in this thesis. Mesh independence study is carried out in Case 1, Case 2, and Case 3 by using three different mesh, a coarse mesh, a medium mesh, and a fine mesh. All three cases use Function Methodology to simulate the wave propagation, which make the wave incident velocity applied to the wave generator available by using a User Defined Function according to the equation of the free surface in Stokes second theory. In addition, damping term is added in the User Define Function by define the viscosity of the water phase to avoid the wave reflection. Case 1, Case 2, and Case 3 are simulated by using the same parameters: wave height 0.14m, wave period 0.8s, water depth 0.5m, and wavelength 1.02m.

Table 2. Mesh Independence Study.

No.	Mesh Used	Method	Wave Height (m)	Wave Period (s)	Wavelength (m)	Water Depth (m)
1	Coarse	FM - Damping	0.14	0.8	1.02	0.5
2	Medium	FM - Damping	0.14	0.8	1.02	0.5
3	Fine	FM - Damping	0.14	0.8	1.02	0.5

In the simulations about mesh independence study, the mesh sizing is the only parameter changed, and remained other mesh settings such as element type and order. By doing this, it will ensure a fair comparison between the simulations. Table 3 shows the difference among mesh independence study cases.

Table 3. Mesh cells and nodes in mesh independence study.

	Coarse	Medium	Fine
Cells	23,040	360,000	5,625,000
Nodes	19,635	382,571	5,487,174

In Case 1, mesh is altered by decreasing the number of elements by an appropriate amount. This coarse mesh has 23,040 hexahedral cells and 19,635 nodes. Figure 9 shows the coarse mesh used in Case 1.

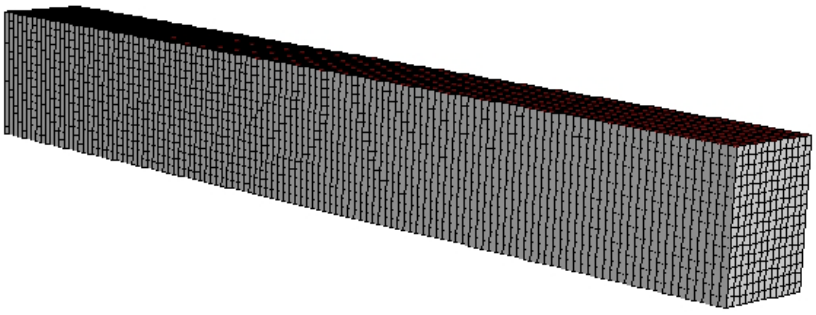

Figure 9. Coarse mesh of wave tank in Case 1.

Figure 10 shows the wave generated in Case 1 by using coarse mesh when the wave has reached the right side of the wall.

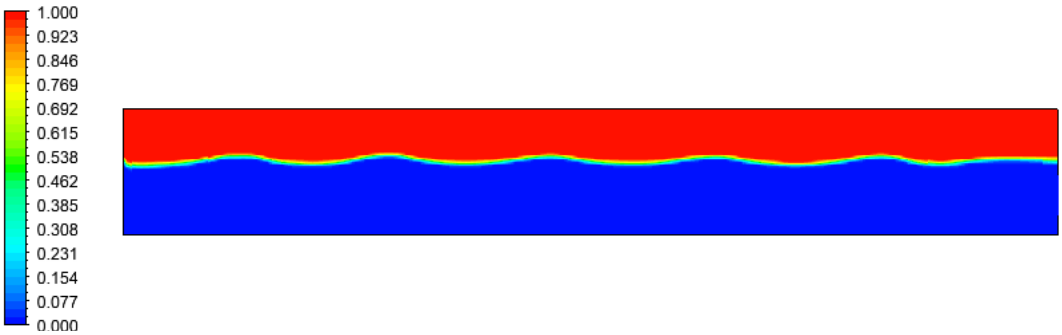

Figure 10. Generation wave using Function Methodology in Case 1.

Figure 11 shows the x-velocity vs. position in Case 1 with decreasing in mesh element. The maximum velocity in x direction is about 0.042m/s. It can be observed that x-velocity did not change much, which means that a coarse mesh cannot capture x-velocity of the wave generated accurately.

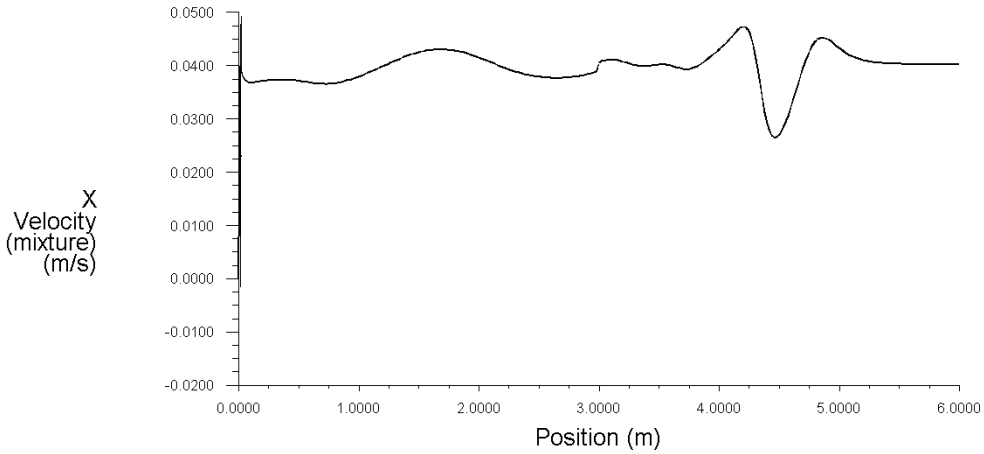

Figure 11. X-velocity vs. Position in Case 1 with damping term added.

In Case 2, the medium mesh has 360,000 hexahedral cells and 382,571 nodes. Figure 12 shows the wave generated by using Function Methodology with damping term added in Case 2.

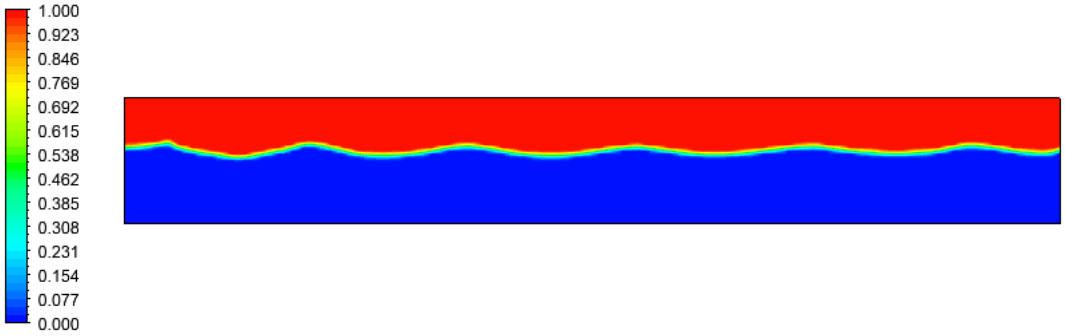

Figure 12. Generation wave using Function Methodology in Case 2.

Figure 13 shows the x-velocity vs. position in Case 2 with damping term added. The maximum velocity in x direction is about 0.05m/s, and the minimum velocity is about -0.05m/s.

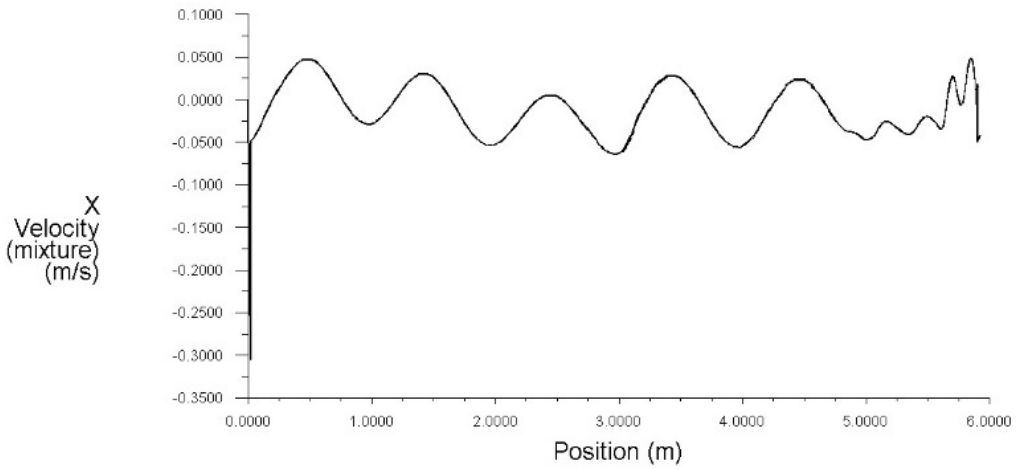

Figure 13. X-velocity vs. Position in Case 2 with damping term added.

In Case 3, the mesh is refined globally to have finer cells throughput the domain. The fine mesh has 5,625,000 hexahedral cells and 5,487,174 nodes. Figure 14 shows the fine mesh used in Case 3, it can be seen that the mesh is finer.

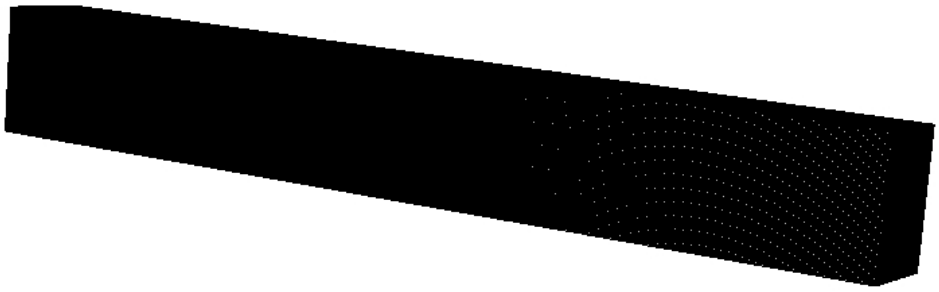

Figure 14. Refined mesh of wave tank in Case 3.

Figure 15 shows the wave generated in Case 3 by using the fine mesh when the wave has reached the right wall of the tank.

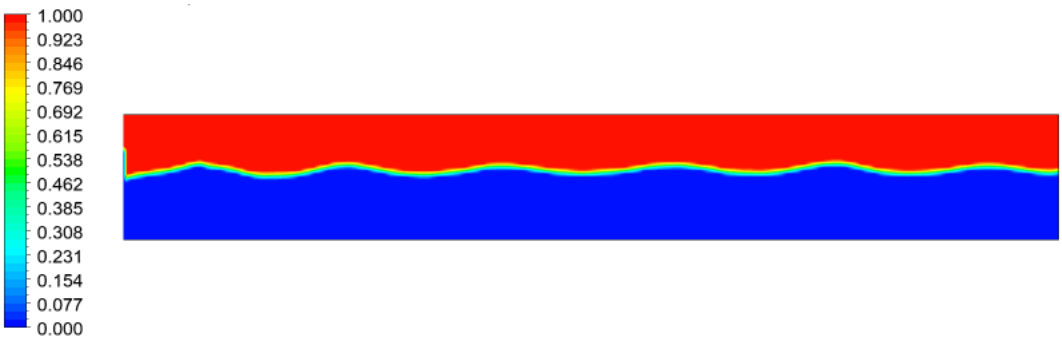

Figure 15. Generation wave using Function Methodology in Case 3.

Figure 16 shows the x-velocity vs. position in Case 3 with increasing in mesh element. It can be observed that the change in x-velocity has a great agreement with the one in Case 2 which refers to the medium mesh. The maximum velocity in x direction is about 0.05m/s, and the minimum velocity is about -0.05m/s.

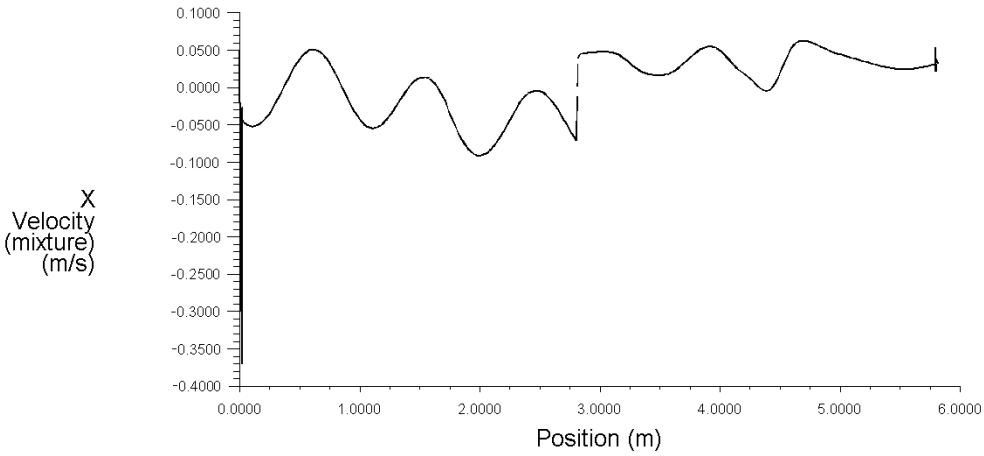

Figure 16. X-velocity vs. Position in Case 3.

3.2.1 Velocity at different position along the wavelength

Figure 17 shows the features of the wave velocity along the wave. Velocity in x direction at different position along the wavelength is analyzed and compared during the mesh independence study.

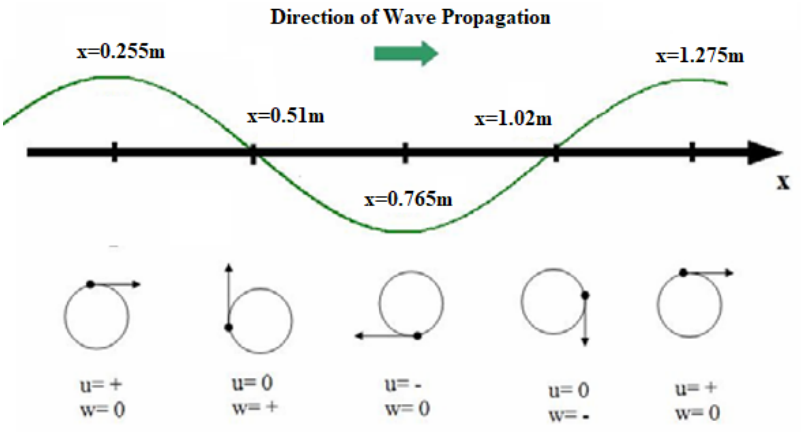

Figure 17. Characteristic of the wave velocity along the wave.

Figure 18 shows the lines created at different locations along the wave in the simulation. Since the wavelength is 1.02m, the positions chosen is $1/4$, $1/2$, $3/4$, 1 and $5/4$ of the wavelength.

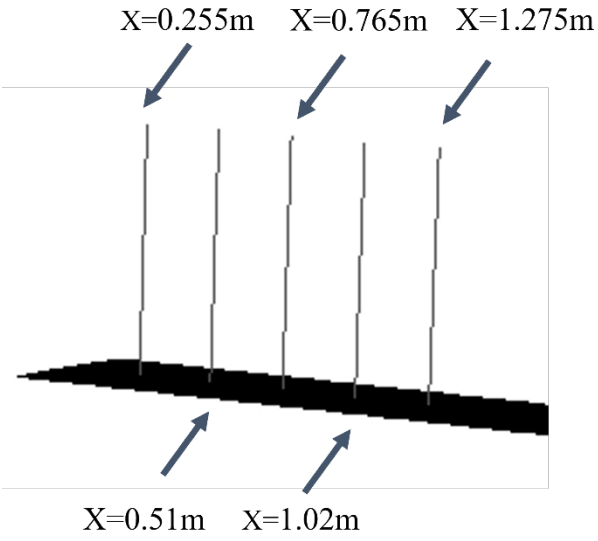

Figure 18. Different locations along the wave.

Figure 19 and Figure 20 shows the results from the reference paper by Gomes et al (2009) [5].

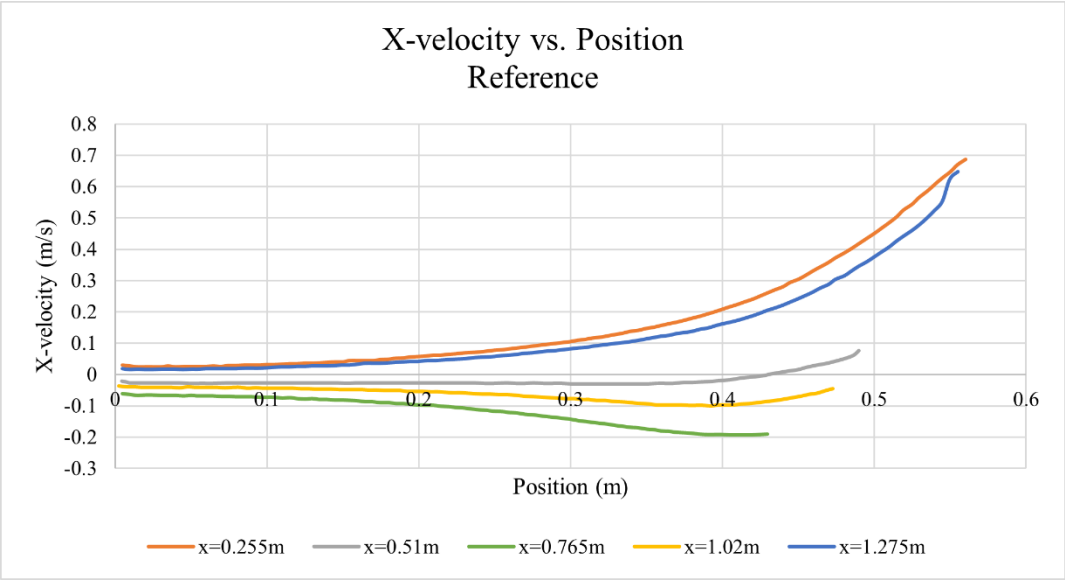

Figure 19. X-velocity vs. Position from reference.

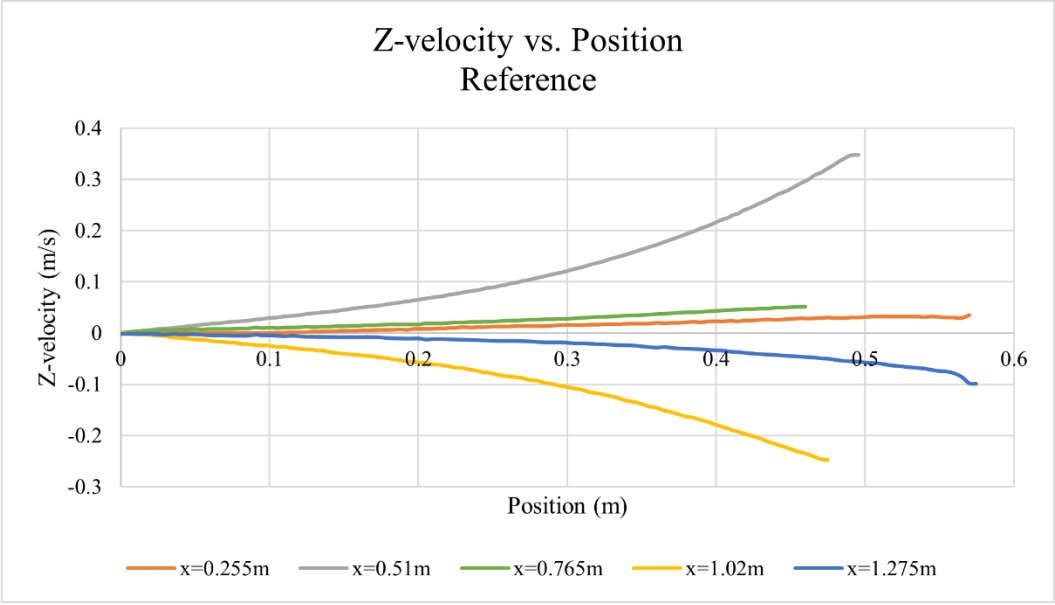

Figure 20. Z-velocity vs. Position from reference.

The velocity in x direction at position x=1.275m vs. Z-coordinate in mesh independence study is shown in Figure 21. Green curve represents the reference solution of x-velocity at position x=1.275m, where at the crest of the wave. The red line refers to the x-velocity by using coarse mesh, the grey one is for the medium mesh, and he blue one illustrates the velocity in x direction by using the fine mesh. It can be concluded that the refined mesh has more accuracy than other mesh, in other words, the coarse mesh gets the less accurate. The x-velocity at position x=1.275m has the maximum velocity since the wave will reach the peak.

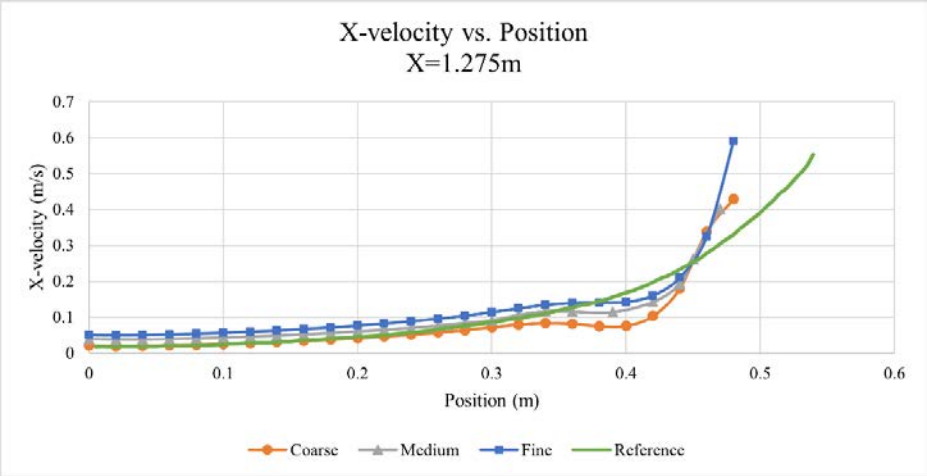

Figure 21. X-velocity at position x=1.275m.

Figure 22 shows the velocity in z direction at position x=1.02m vs. Z-coordinate. It can be observed that fine mesh has the more precise result compared with the reference solution. On the other hands, the coarse mesh has a high error rate. At position x=1.02m, where at the air-water interface, the velocity in z direction in negative.

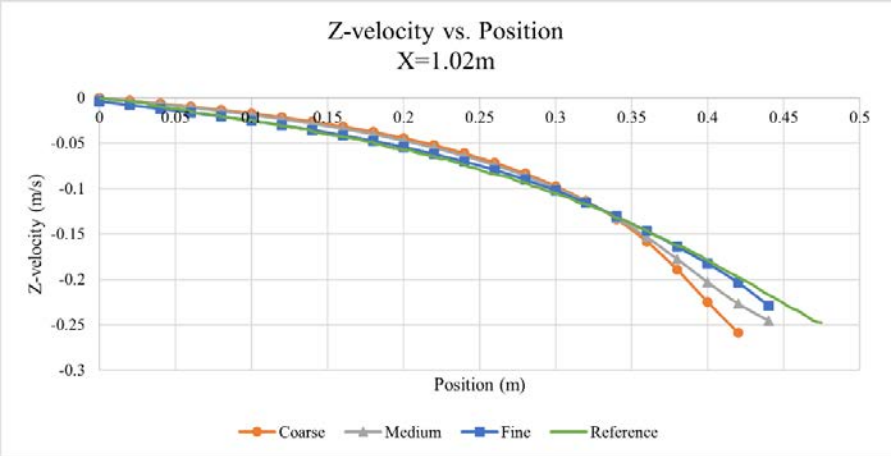

Figure 22. Z-velocity at position x=1.275m.

From Figure 21, it can be noticed that the main difference of x-velocity among three cases and reference solution is rang from Z=0.34m to Z= 0.45m. From Figure 22, it can be seen that the main difference of z-velocity is range from Z=0.34m to Z=0.45m. Table 4 and Table 5 show the percentage error of the velocity in x and in z direction. It can be noticed that the coarse mesh has the biggest error, the fine mesh has the least error.

Table 4. Error of x-velocity in mesh independence study.

X-velocity (m/s) / Position (m)	Error (%)		
	Coarse	Medium	Fine
Z=0.35	29.2	2.5	-1.8
Z=0.40	35.5	23.1	14.8
Z=0.44	22.4	17.4	9.6

Table 5. Error of z-velocity in mesh independence study.

Z-velocity (m/s) / Position (m)	Error (%)		
	Coarse	Medium	Fine
Z=0.35	4.6	2.8	0.1
Z=0.40	22.7	10.8	2.2
Z=0.425	31.4	8.6	3.4

It can be concluded that the coarse mesh has a large difference with the medium mesh and fine mesh. It can be assumed that a fine mesh has the similar accuracy for the solution with the medium mesh, but it will take more time to finish the simulation. To rephrase it, given a degree of precision for the solution, the medium mesh utilized is good enough to accomplish that accuracy at the expense of minimum potential computational power and to capture all the necessary flow features, and their gradients.

3.3 Numerical Simulations

Table 6 shows the numerical simulations performed with two method and different wave parameter.

Table 6. Numerical simulations.

No.	Method	Wave Height (m)	Wave Period (s)	Wavelength (m)	Water Depth (m)
1	FM	0.14	0.8	1.02	0.5
2	MM	0.14	0.8	1.02	0.5
3	FM	0.14	1.5	2.8	0.5
4	MM	0.14	1.5	2.8	0.5
5	FM – Damping	0.14	1.5	2.8	0.5

3.4 Baseline Simulations

Function Methodology is used in Case 1 to generate the wave but without damping term added. Case 2 choose to use Mobile Methodology to generate the wave propagation, which allows the moving wall boundary condition applied to a wave generator to make it moves like a piston. Case 1 and Case 2 are carried out by using the parameter wave height 0.14m, wave period 0.8s, depth of the tank 0.5m, and wavelength 1.02m.

Case 1 and Case 2 are developed with the same parameters, but using different methodology, one is Function Methodology, and the other one is Mobile Methodology. Both cases are simulated without the damping term added in the momentum equation. In these two cases, wave height is 0.14m, wave period is 0.8s, water depth is 0.5m, and wavelength is 1.02m. In addition, 0.5m of the bottom is the water depth, and the other 0.3m is the air depth.

Figure 23, Figure 24, Figure 25, and Figure 26 present the interaction between air, which is red in the top of the wave tank, and water, which is blue part in the wave tank in Case 1 and Case 2, respectively. Figure 23 shows the wave generated by using Function Methodology in Case 1 when the time is 6s, at this time the wave has not reached the end of the tank.

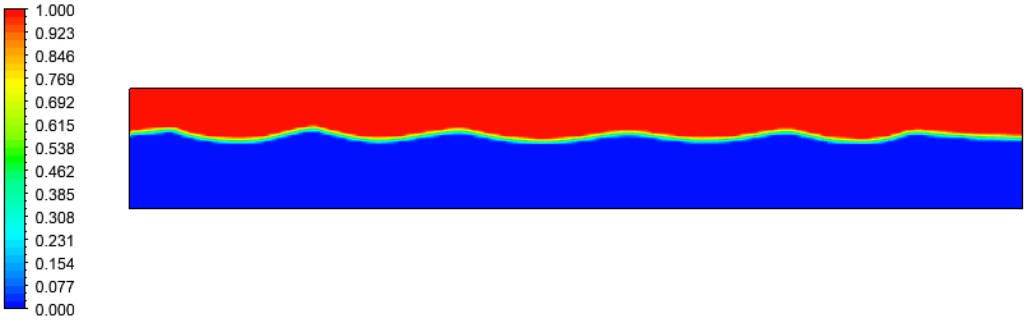

Figure 23. Generation wave using Function Methodology in Case 1 when t=6s.

Figure 24 shows the wave generated in Case 1 when the time is 16s, at which time the wave has already reached the right wall of the tank, which lead to the backflow phenomena.

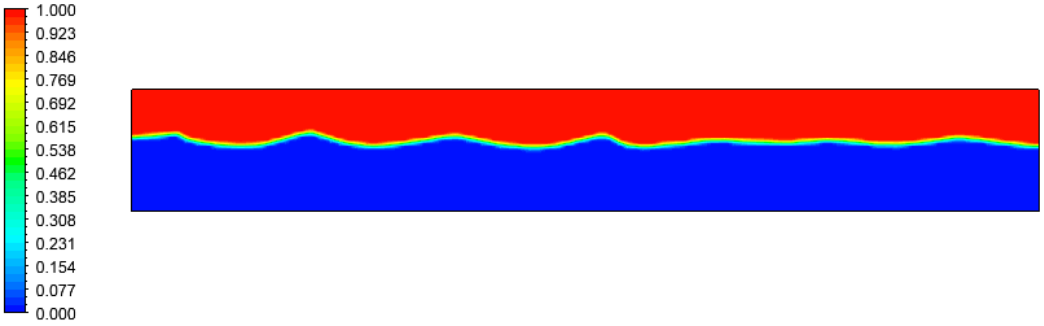

Figure 24. Generation wave using Function Methodology in Case 1 when t=14s.

Figure 25 shows the wave generated by using Mobile Methodology in Case 2 when the time is 6s, and the wave has not reached the end of the tank.

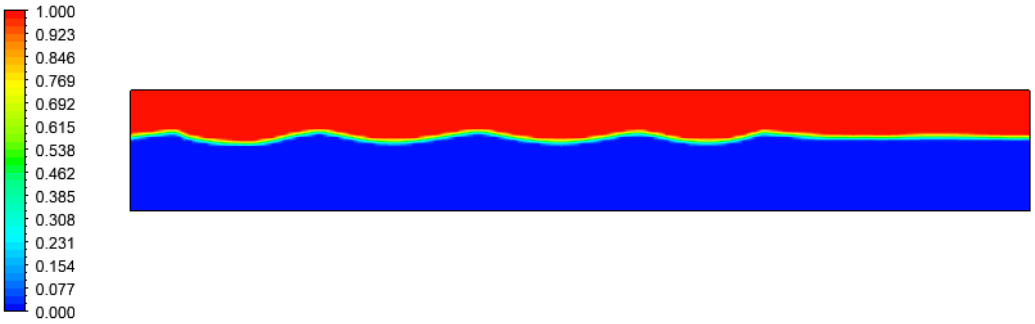

Figure 25. Generation wave using Mobile Methodology in Case 2 when t=6s.

Figure 26 shows the wave generated in Case 2 when the time is 14s, and the wave has already reached the right wall of the tank, which generated the reflection of the wave.

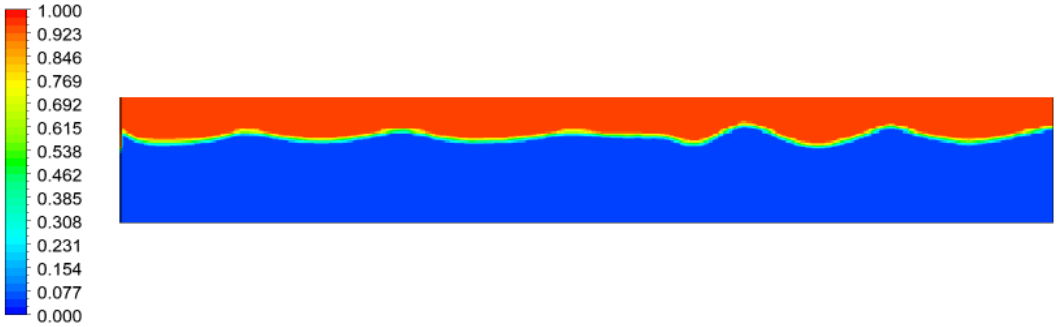

Figure 26. Generation wave using Mobile Methodology in Case 2 when t=14s.

Figure 23 and Figure 25 shows show the suggested numerical model's capacity to create regular waves in the wave tank, and the waves generated appear to be quite comparable. The wave propagations in Case 1 and Case 2 and are given the fact that it can generate waves with the preferred physical characteristics, which means the simulations conducted by both Function Methodology and Mobile Methodology are appropriate.

In Figure 24 and Figure 26, there are wave reflection in the end of the wave tank region, which can interfere with the generated waves. A damping sink term was explored adding in the momentum equation in User Define Function to avoid wave reflection.

In Figure 27, it shows three curves, representing experimental curves generated by the simulation and the analytical curve of amplitude. From the figure, the height of the wave is 0.14m in both Function Methodology and Mobile Methodology. The two curves have a high degree of similarity with the analytical curve, which means both Function Methodology and Mobile Methodology are possible to simulate the wave propagation.

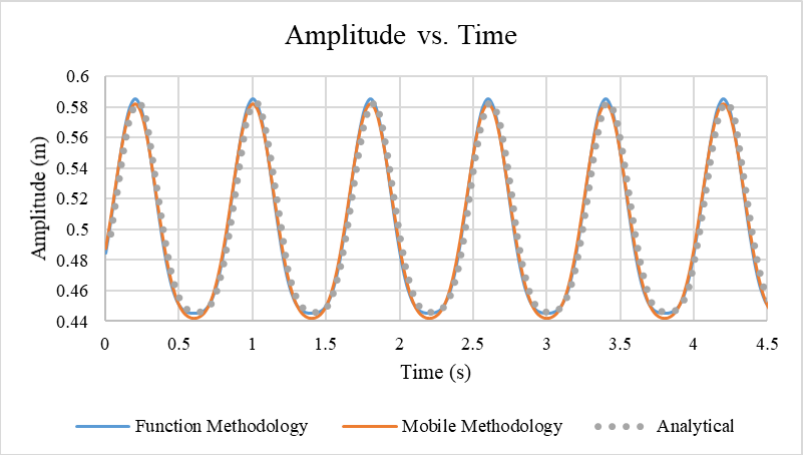

Figure 27. Amplitude of the Wave at Position x=0m.

Figure 28 shows two curves about x-velocity at position x=0m, blue line represents the numerical result, and the grey one refers to analytical result. The x-velocity from numerical simulation is about 0.5m/s, the analytical result is about 0.65m/s. It can be observed that Function Methodology has a good agreement with the analytical result.

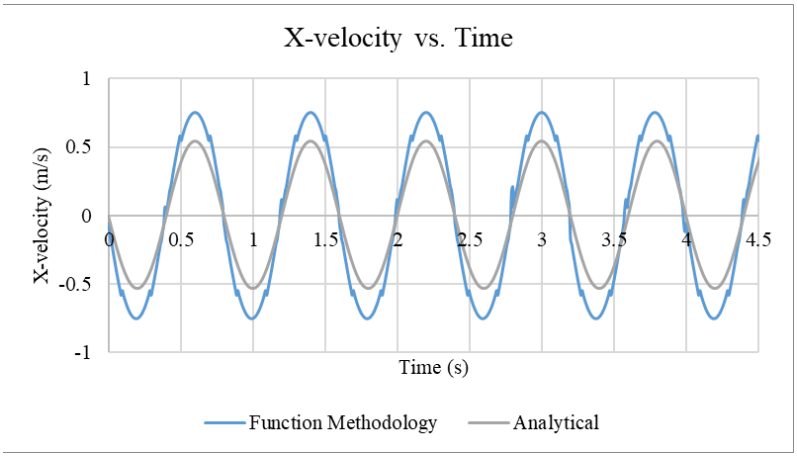

Figure 28. X-velocity at Position x=0m using Function Methodology in Case 1.

In Figure 29, two curves about z-velocity at position x=0m are shown. Blue line represents the numerical result, and the grey one refers to analytical result. The x-velocity from Function Methodology is about 0.1m/s, in addition, the analytical result is about 0.1m/s. It can be observed that Function Methodology has a great agreement with the analytical result.

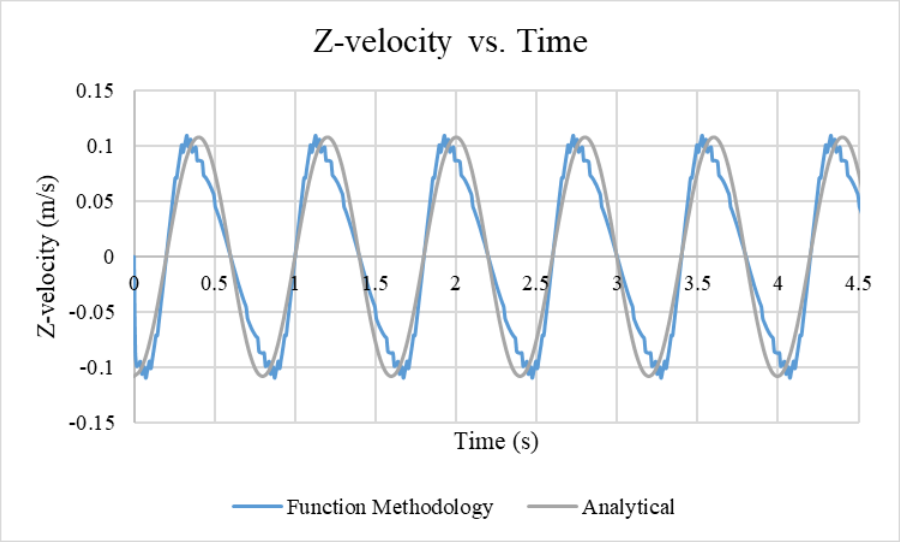

Figure 29. Z-velocity at Position x=0m using Function Methodology in Case 1.

Figure 30 shows two curves about x-velocity at position x=0m, red line illustrates the numerical result, and the grey one refers to analytical result. It can be observed that there was a process for Mobile Methodology to generate the wave at the beginning of the simulation. The x-velocity from numerical result is about 0.5m/s, and the analytical result is about 0.6m/s. In other words, Mobile Methodology has a great agreement with the analytical result as well.

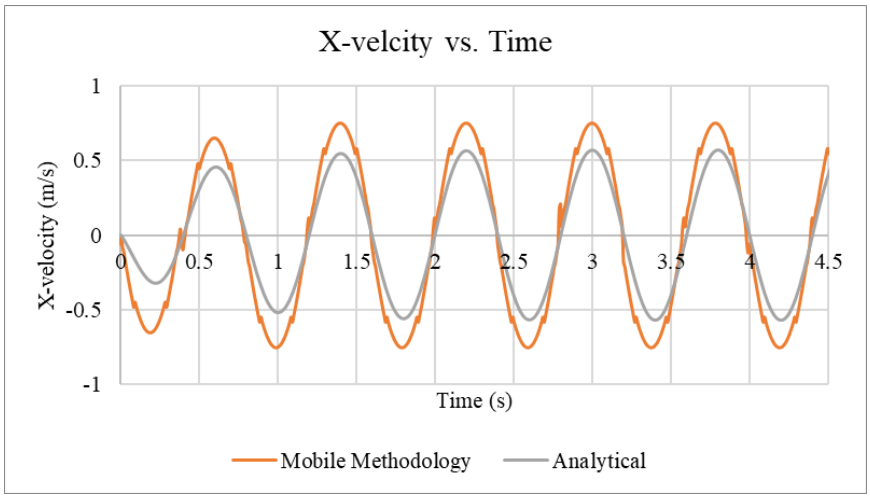

Figure 30. X-velocity at Position x=0m using Mobile Methodology in Case 2.

The curves about velocity in x direction at position x=0m generated by two different numerical method are shown in Figure 31. During the first wave period, Mobile Methodology shows a process generate the wave by applying User Define Function to the wave generator to make it moving like a piston during the beginning of the simulation. It can be observed that after one wave period, two curves are almost the same.

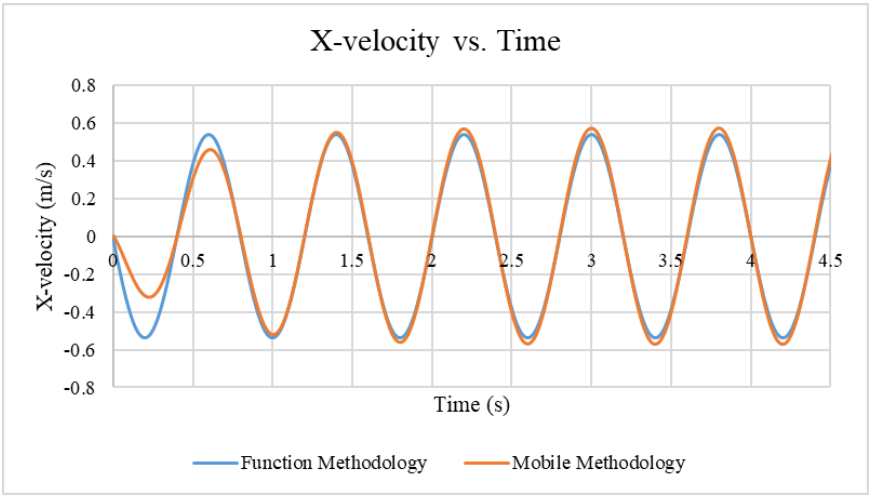

Figure 31. X-velocity at Position x=0m.

In Figure 32 and Figure 33, the contour of the velocity in x direction is shown by using Function Methodology in Case 1. In Figure 32, when time is 6s, it can easily be observed that the

velocity of the connection between water and air is the biggest, and the velocity decreases to the sides of the tank. The maximum x-velocity occurs at the crest and the trough of the wave, while their directions are in opposite directions.

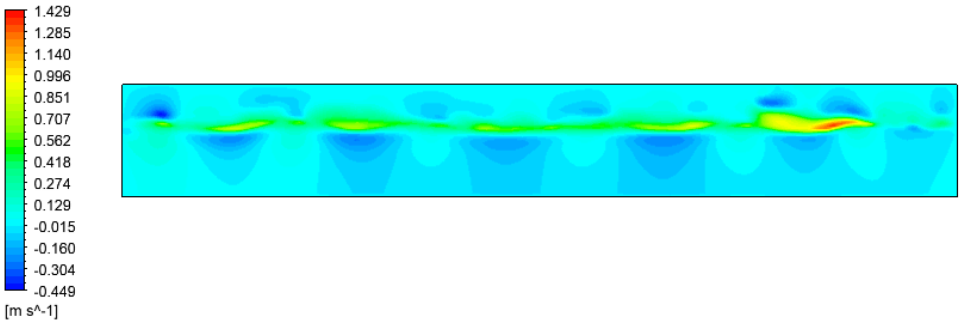

Figure 32. Topology of velocity in x direction using Function Methodology in Case 1 when t=6s.

In Figure 33, when time is 14s, there are backflows generated at the end of the wave tank, the waves are reflected by a structure from interfering with the generated waves.

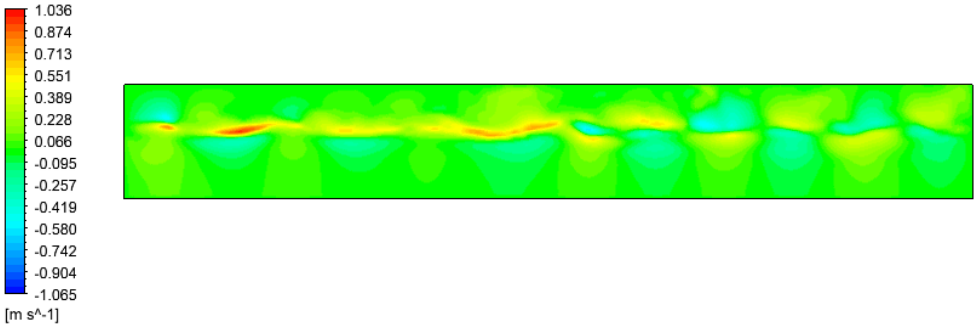

Figure 33. Topology of velocity in x direction using Function Methodology in Case 1 when t=14s.

Velocity in x direction in Case 1 at different locations vs. Z-coordinate, where x=0.255m, x=0.51m, and x=0.765m are shown in Figure 34. It can be exemplified that Function Methodology can have the possibility to generate the desired wave since the numerical results have a great accuracy with the reference solutions. At x=0.255m, the wave has reached the peak, which means it has the maximum x-velocity. At x=0.51m, where at the air-water interface, the velocity in x

direction is almost equals to zero. At x=0.765m, where at the trough of the wave, which means the minimum velocity is obtained at this location.

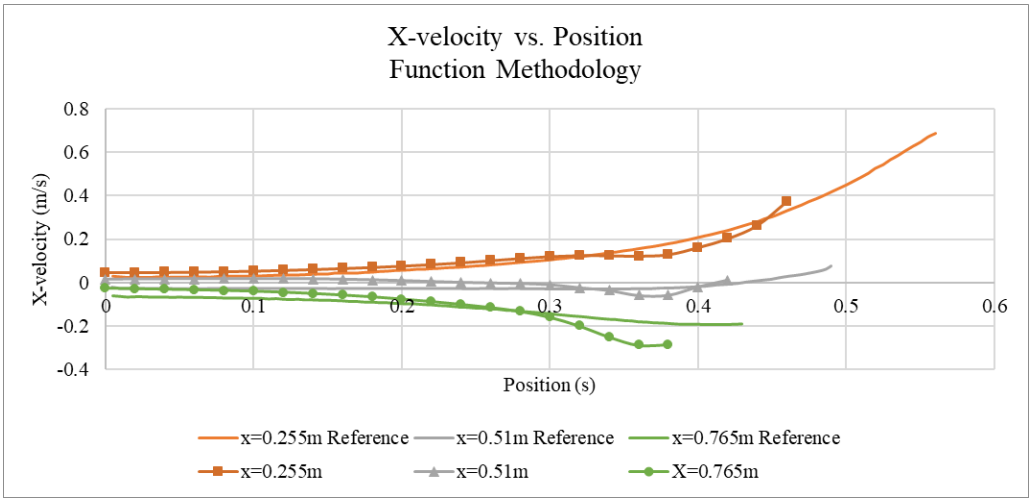

Figure 34. X-velocity at different positions in Case 1.

Figure 35 shows the velocity in z direction at different position x=0.255m, x=0.51m, and x=1.02m in Case 1 vs. Z-coordinate. At x=0. 255m, the wave achieved the highest point of the wave, which leads to velocity in z direction nearly equals to zero. At x=0.51m, and =1.02m, where at the air-water interface, it has the maximum z-velocity, but with the opposite directions. Which is because at x=0.51m, the z-velocity is in the positive z direction, and at x=1.02m, the z-velocity is in the negative z direction.

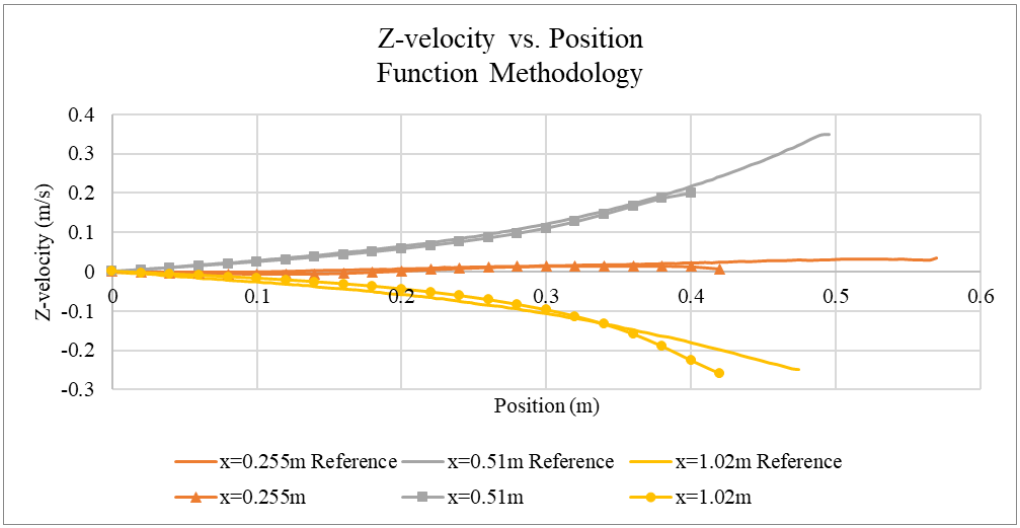

Figure 35. Z-velocity at different positions in Case 1.

The percentage error of x-velocity and z-velocity is shown in Table 7 and Table 8. It can be concluded that the results by using Function Methodology have a reasonable agreement with the reference solutions.

Table 7. Error of x-velocity in Case 1.

X-velocity (m/s) / Position (m)	Error (%)		
	X=0.255m	X=0.51m	X=0.765m
Z=0.20	-5.1	-6.3	-3.2
Z=0.30	-3.9	-4.1	-4.3
Z=0.40	12.3	11.4	15.3

Table 8. Error of z-velocity in Case 1.

Z-velocity (m/s) / Position (m)	Error (%)		
	X=0.255m	X=0.51m	X=1.02m
Z=0.20	0.3	0.3	-0.8
Z=0.30	0.2	0.9	-1.3
Z=0.40	5.1	5.3	20.2

In Figure 36 and Figure 37, the contour of the velocity in x direction is shown by using Mobile Methodology in Case 2. When time is 6s, the wave has not reached the right wall of the tank, the velocity in x direction is similar to the one shown in Figure 32 in Case 1 using Function Methodology.

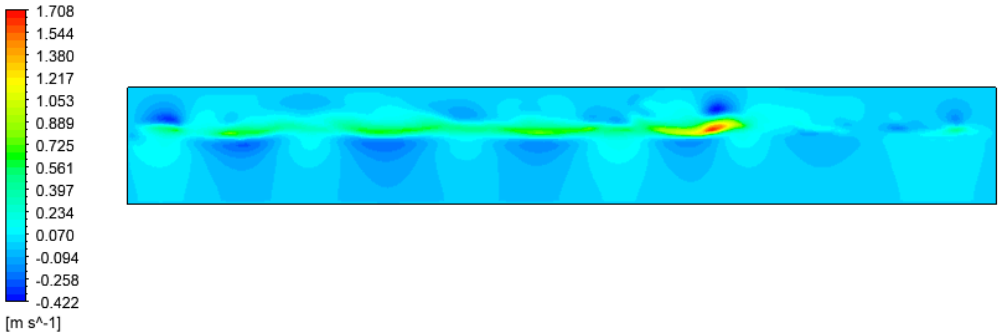

Figure 36. Topology of velocity in x direction using Mobile Methodology in Case 2 when t=6s.

In Figure 37, the wave has reached the end of the tank, which caused the backflow and affected the velocity of generated waves.

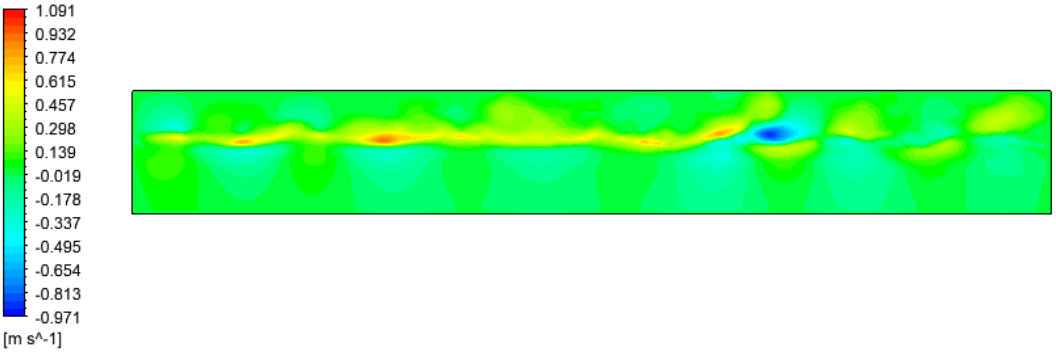

Figure 37. Topology of velocity in x direction using Mobile Methodology in Case 2 when t=14s.

Figure 38 and Figure 39 shown that the simulation results have a great agreement with the reference solutions, which means that Mobile Methodology has the feasibility of generating the wave.

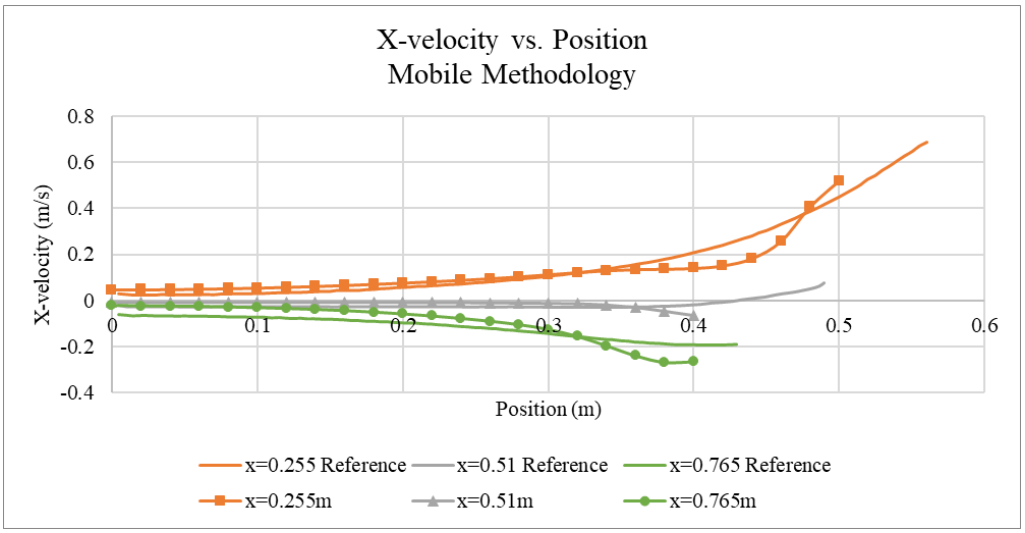

Figure 38. X-velocity at different positions in Case 2.

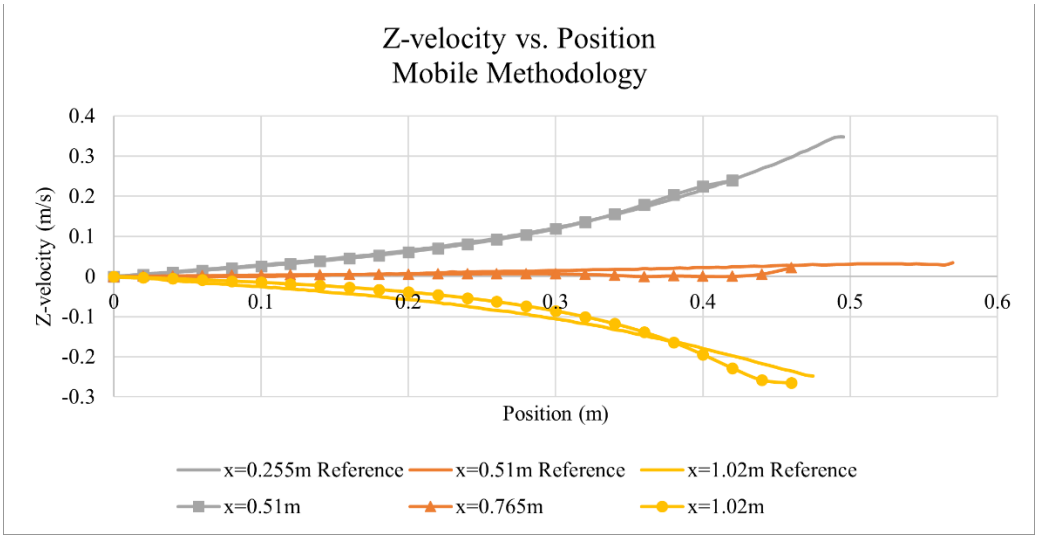

Figure 39. X-velocity at different positions in Case 2.

In Table 9 and Table 10, the percentage error of x-velocity and z-velocity in Case 2 is shown. It can be noticed that the results from Mobile Methodology match with the reference results.

Table 9. Error of x-velocity in Case 2.

X-velocity (m/s) / Position (m)	Error (%)		
	X=0.255m	X=0.51m	X=0.765m
Z=0.24	-2.2	-2.2	-3.5
Z=0.30	0.4	-1.1	-2.1
Z=0.36	6.7	8.3	10.7

Table 10. Error of z-velocity in Case 2.

Z-velocity (m/s) / Position (m)	Error (%)		
	X=0.255m	X=0.51m	X=1.02m
Z=0.20	0.1	0.1	-4.3
Z=0.30	0.1	1.4	-3.7
Z=0.40	-1.4	3.1	2.4

3.5 Simulations on Changing Wave Period and Wavelength

After studying the two methods to generate the wave, detail studies are carried out by changing the wave parameters. From Equation 16, Equation 17 on velocity components by using Function Methodology, and Equation 20 on wave velocity by using Mobile Methodology, it can be concluded that the velocity is related to wave period and wavelength. Case 3 uses Function Methodology without damping term to analyze the wave propagation. Case 4 uses Mobile Methodology without damping term to investigate the propagation of the wave. Maintain the same wave height as 0.14m and water depth 0.5m, increase the wave period to 1.5s and wavelength to 2.8m. Use both Function Methodology and Mobile Methodology to simulate the wave, and compare them with previous cases to study the wave behavior.

The waves generated in the wave tank when time is 8s and the wave has not reached the end of the tank are shown in Figure 40 and Figure 41. It can be seen that amplitude is about to be

the similar, but the wavelength is larger than the one in Case 1 and Case 2. To produce waves in a container partially filled with liquid and open to the atmosphere, the oscillating motion of the wall can be used. By setting appropriate frequencies and amplitudes, flat slip waves can be generated.

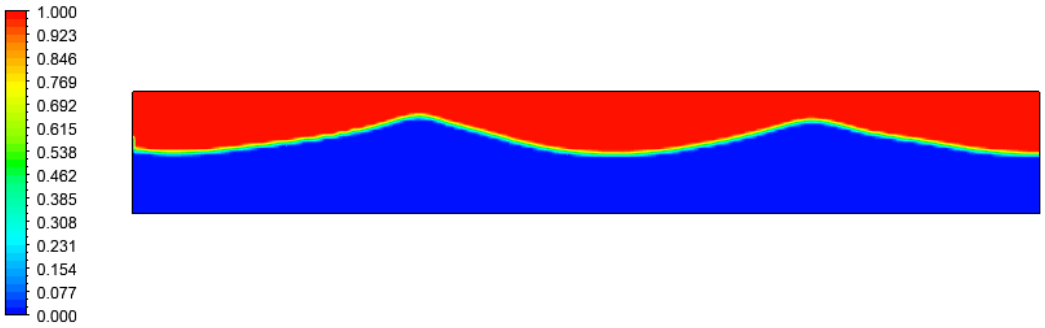

Figure 40. Generation wave using Function Methodology in Case 3 when t=8s.

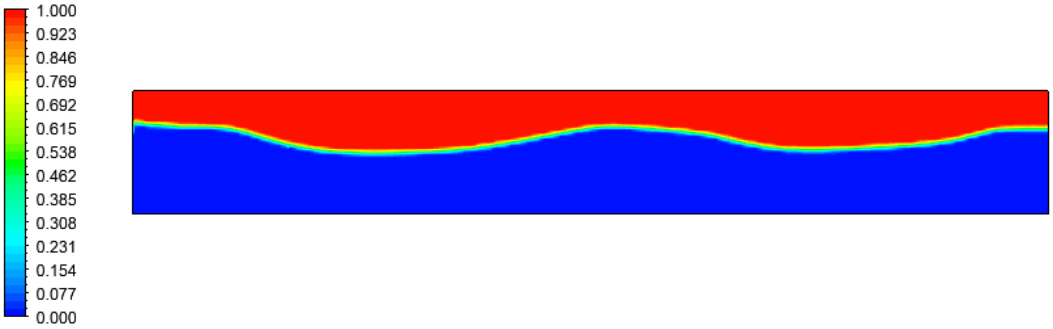

Figure 41. Generation wave using Mobile Methodology in Case 4 when t=8s.

Figure 42 shows the velocity in x direction at position x=0m. Blue line signifies the numerical result, and the grey one refers to the analytical result. X-velocity in numerical simulation is about 0.8m/s, and the analytical result is about 0.85m/s. It can be observed that the numerical

curve by using Function Methodology, which is color in blue, has a reasonable agreement with the analytical result, which is color in grey.

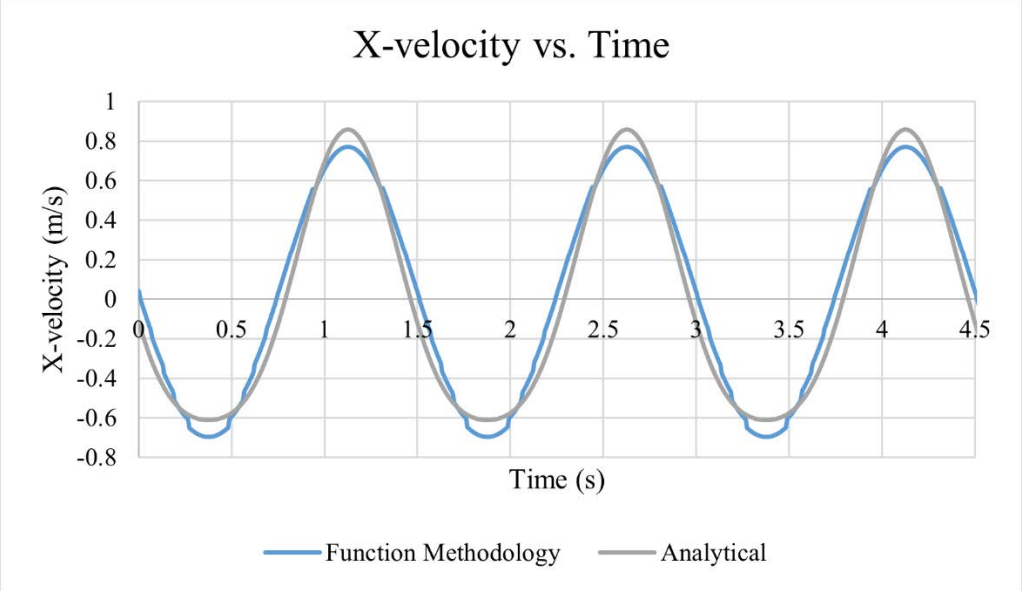

Figure 42. X-velocity at Position x=0m using Function Methodology.

In Figure 43, it can be concluded that the simulation result of Mobile Methodology matched with the analytical result.

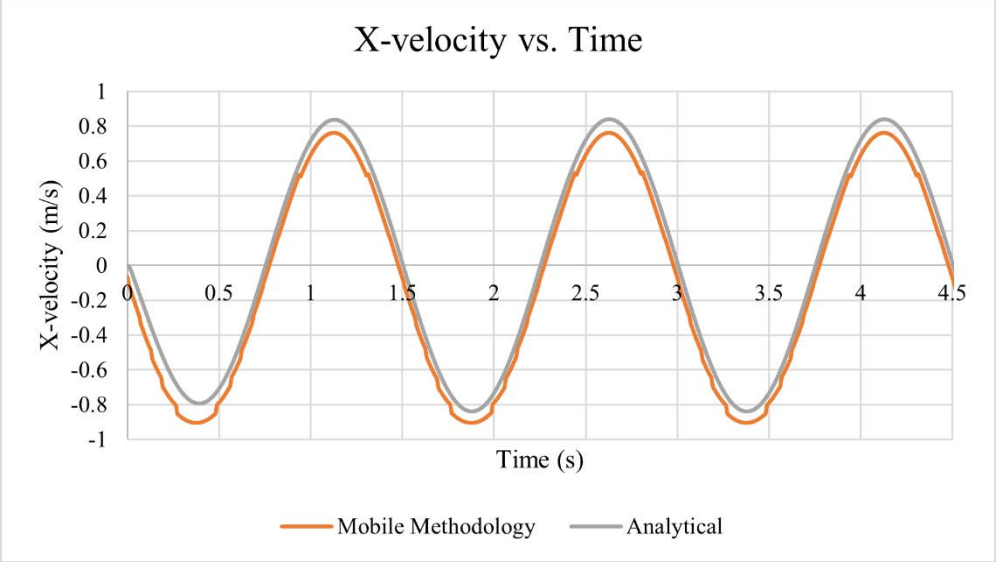

Figure 43. X-velocity at Position x=0m using Mobile Methodology.

The curves about velocity in x direction at position x=0m are shown in Figure 44 generated by two different numerical method with changing in wave period and wavelength. It can be observed that Mobile Methodology can obtain maximum velocity as 0.75m/s, and minimum velocity as -0.9m/s. The velocity using two methodologies shows good agreement with each other.

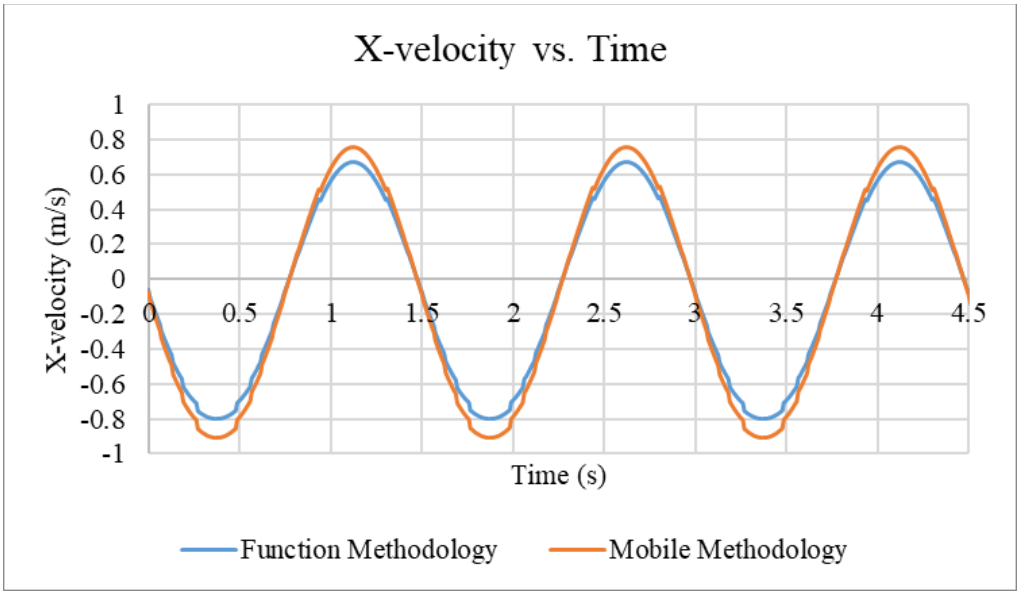

Figure 44. X-velocity at position x=0m.

In Figure 45, it shows that two velocities in x direction with different wavelength 1.02m and 2.8m using Function Methodology. From Equation 16 and Equation 17 about velocity components, it can be concluded that x-velocity is associated with wave period and wavelength. Increasing in wave period and wavelength in Case 3 make the velocity in x direction obtain higher and lower velocities, compared with Case 1 which using Function Methodology with wavelength 1.02m. When the wavelength is 1.02m, x-velocity is range from -0.5 m/s to 0.5m/s. After increasing the wavelength to 2.8m, x-velocity is range from -0.8m/s to 0.7m/s. At position x=0m, the time for the molecules to complete cycle is 0.8s and then is increased to 1.5s.

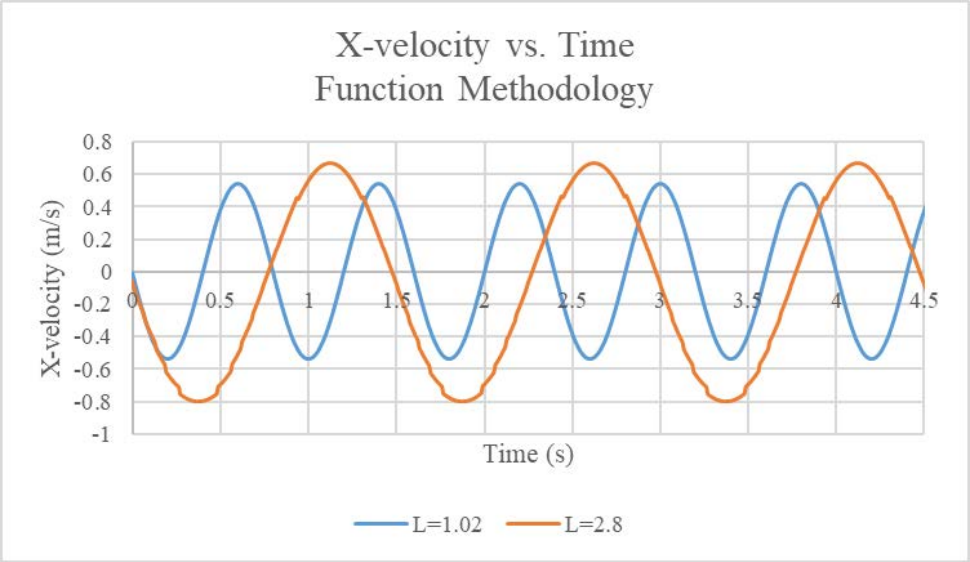

Figure 45. X-velocity at position x=0m using Function Methodology.

In Figure 46, it shows that two velocities in x direction with different wavelength 1.02m and 2.8m using Mobile Methodology. From Equation 20 about wave velocity, it can be known that x-velocity is related to wave period and wavelength. When the wavelength is 1.02m, x-velocity is range from -0.5m/s to 0.5m/s, the same as the simulation using Function Methodology in Case 1, after increasing the wavelength to 2.8m, x-velocity is range from -0.8m/s to 0.8m/s. At position x=0m, the time for the molecules to complete cycle is 0.8s and then is increased to 1.5s.

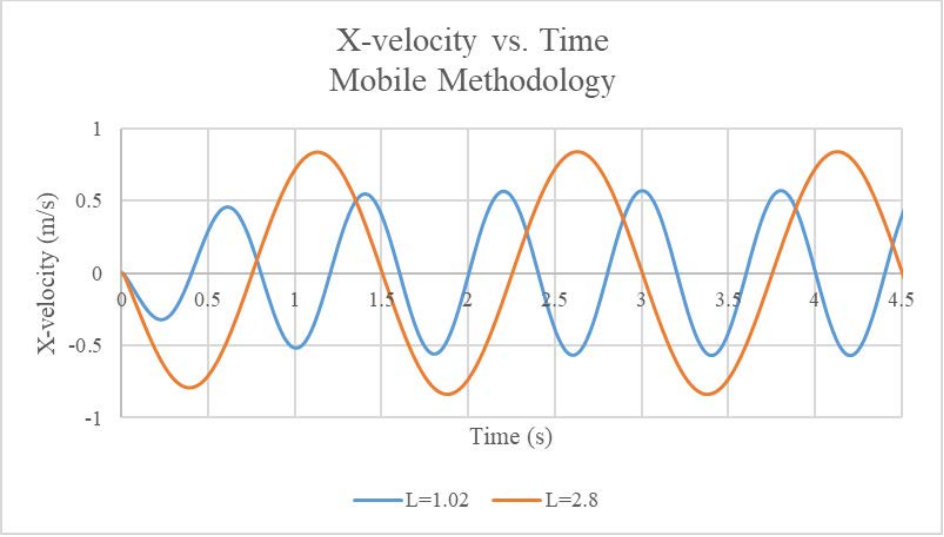

Figure 46. X-velocity at position x=0m using Mobile Methodology.

In simulations on changing both wave period and wavelength, the combined effect is studied. In Figure 47, it shows three curves. The blue line represents baseline simulation, wavelength equals to 1.02m, and wave period equals to 0.8s. The red line refers to simulation on increasing both wavelength and wave period. The green one shows the one only increases the wavelength form 1.02m to 2.8m. It can be concluded that, if only increase the wavelength, compare the blue line with the green line, the velocity will be increased. While if only increase the wave period, compare the red line with the green line, the velocity will decrease. If both the wavelength and the period are increased, the combined effect of the increase in velocity will be reduced.

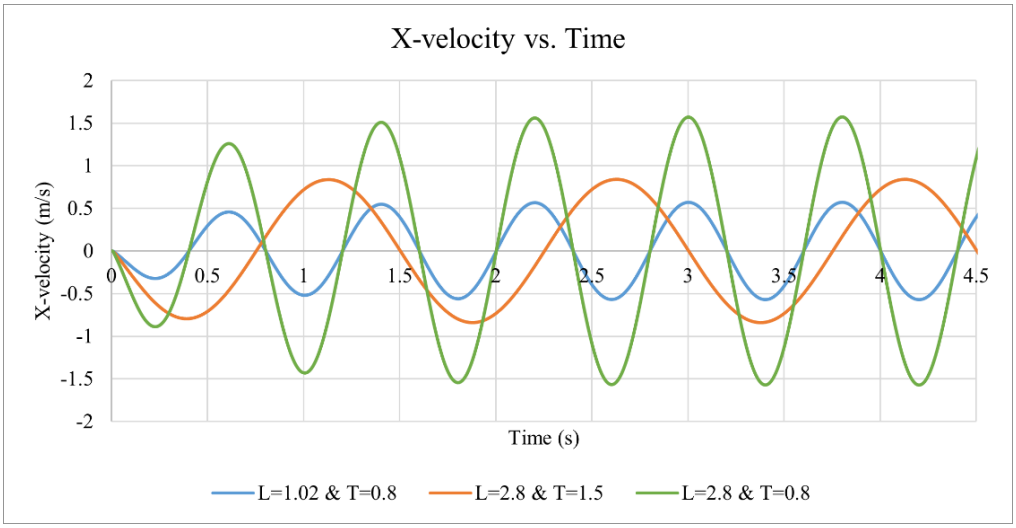

Figure 47. X-velocity vs. Time.

In Figure 48 and Figure 49, the topology of the velocity in x direction is shown by using Function Methodology in Case 3 and Mobile Methodology in Case 4. The wavelength is bigger compared to the one shown in Figure 32 and Figure 36. Compared to the gas phase, the velocity was much larger in the liquid phase when the wave was above the mean sea level. In other words, compared to the gas phase, when the wave was below the mean sea level, the velocity was much smaller in the liquid phase.

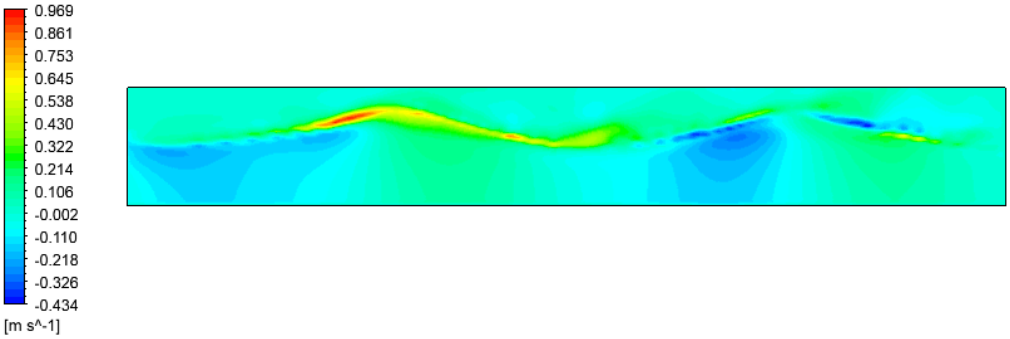

Figure 48. Topology of velocity in x direction using Function Methodology in Case 3 when t=8s.

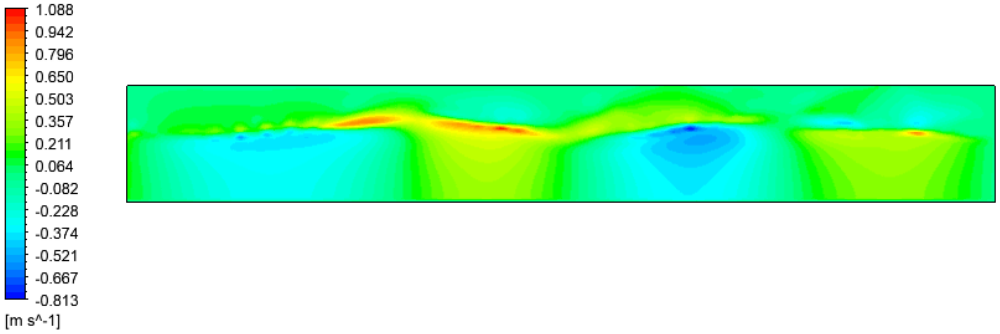

Figure 49. Topology of velocity in x direction using Mobile Methodology in Case 4 when t=8s.

3.6 Simulations on Adding Damping Term

To define the properties of the materials, DEFINE_PROPERTY in ANSYS FLUENT for single-phase and multiphase flows is used. Some of the properties can be customized using DEFINE_PROPERTY, such as viscosity, density, laminar flow speed, thermal conductivity, scattering coefficients, and absorption etc [19].

In previous simulation, when the wave is propagated to the end of the tank, it will cause reflection of the wave, since the right wall of the tank is defined as a wall. In real ocean environment, the backflow phenomena would not happen. For better simulation ocean wave, it is necessary to reduce the backflow in the ocean wave simulation, a damping sink term is added to specify the viscosity of the water phase. The viscosity is very high when the flow is at the end of the wave tank so that the wave reflection can be avoided in the wave simulation. Figure 50 shows how molecular viscosity of water change with position.

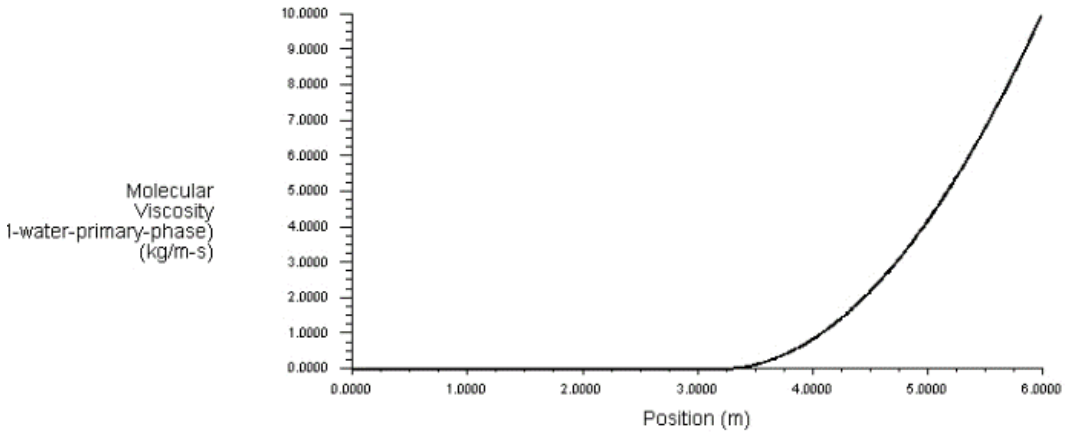

Figure 50. The molecular viscosity of water.

The air volume fractions in the wave tank are shown in Figure 51 and Figure 52. It can be clearly noticed that there was no backflow in the wave simulations at the end of the wave tank, which means the damping term included in the momentum equation was work successfully. Both simulations on adding damping term are using Function Methodology but with different parameters. Figure 51 shows the result in Case 1 in mesh independence study, the simulation is carried out by using the parameter wave height 0.14m, wave period 0.8s, depth of the tank 0.5m, and wavelength 1.02m. In Figure 52, Case 5 is carried out by changing the parameters, wave height 0.14m, wave period 1.5s, depth of the tank 0.5m, and wavelength 2.8m. With adding the damping term in Case 1 and Case 5, the wave propagation is much more reasonable with the result of avoiding the wave reflection.

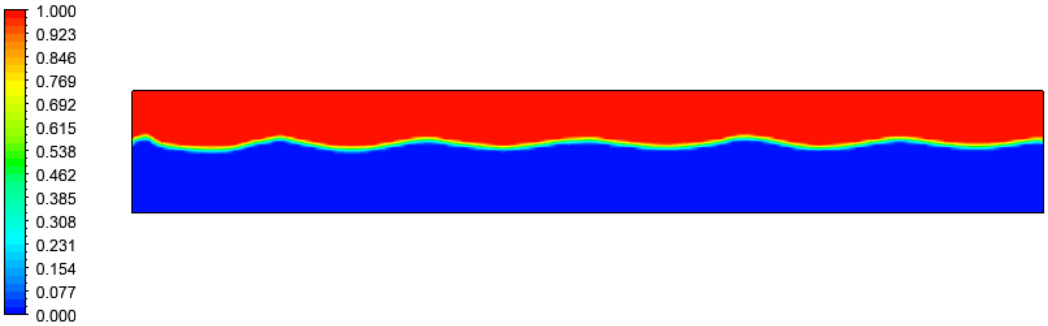

Figure 51. Generation wave using Function Methodology in Case 1 in mesh independence study.

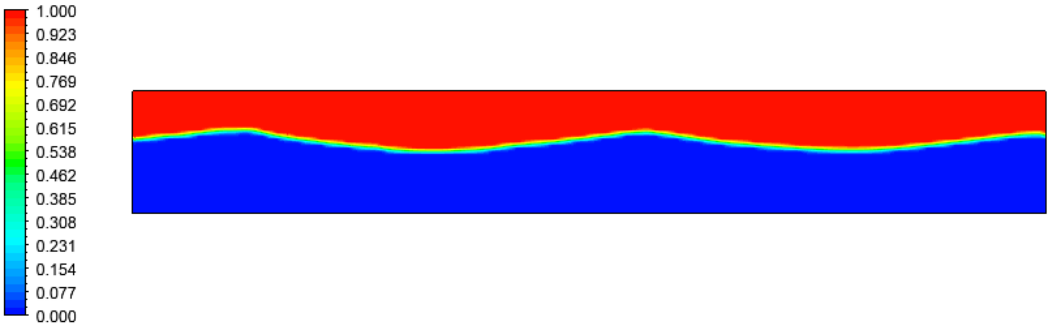

Figure 52. Generation wave using Function Methodology in Case 2.

In Figure 53 and Figure 54, the topology of x-velocity using Mobile Methodology with damping term added in the momentum equation in User Define Function in Case 1 and Case 5 is shown. Compared with the cases without adding damping term, without the wave reflection, the wave propagates to the right of the wave tank, which make the x-velocity at the end of the wave tank seems more reasonable.

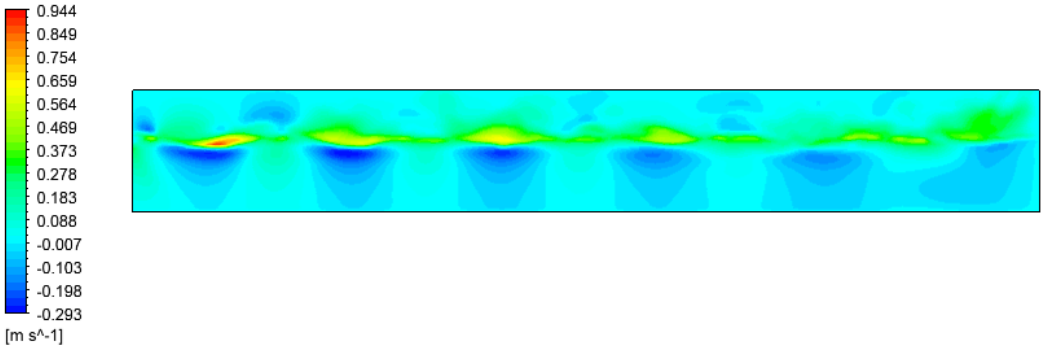

Figure 53. Topology of velocity in x direction using Function Methodology with damping term added in Case 1.

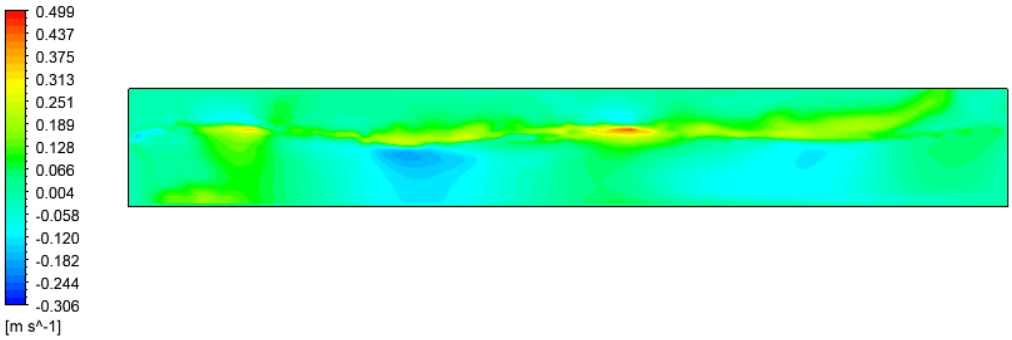

Figure 54. Topology of velocity in x direction using Function Methodology with damping term added in Case 2.

3.6.1 X-velocity vs. Position

Figure 55 and Figure 56 represent x-velocity vs. position in previous case using Function Methodology without damping term added and in Case 1 with damping term added, respectively. The time chosen is after the wave get reflection. In both cases, the simulations are carried out by using the same parameter wave height 0.14m, wave period 0.8s, water depth 0.5m, and wavelength 1.02m.

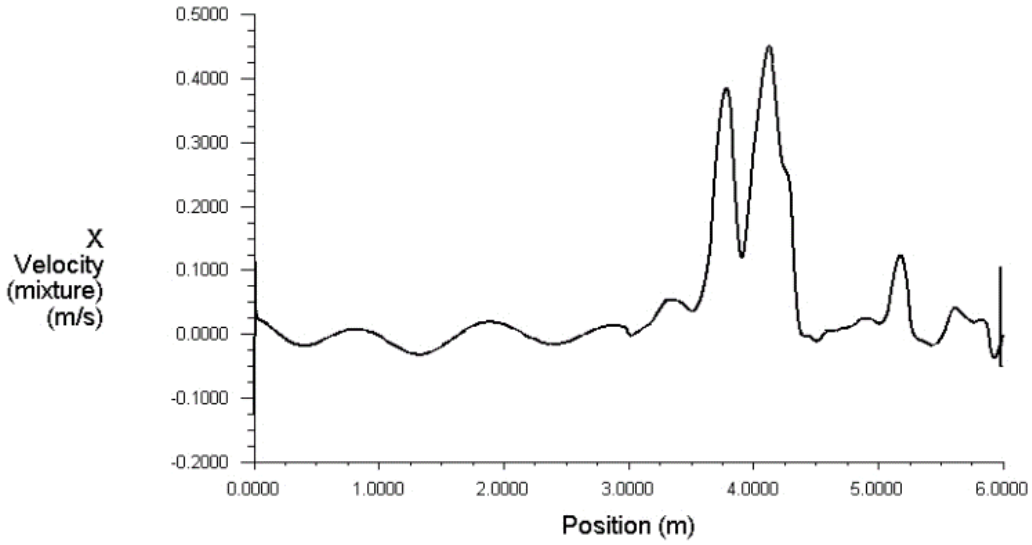

Figure 55. X-velocity vs. Position in case without damping term added.

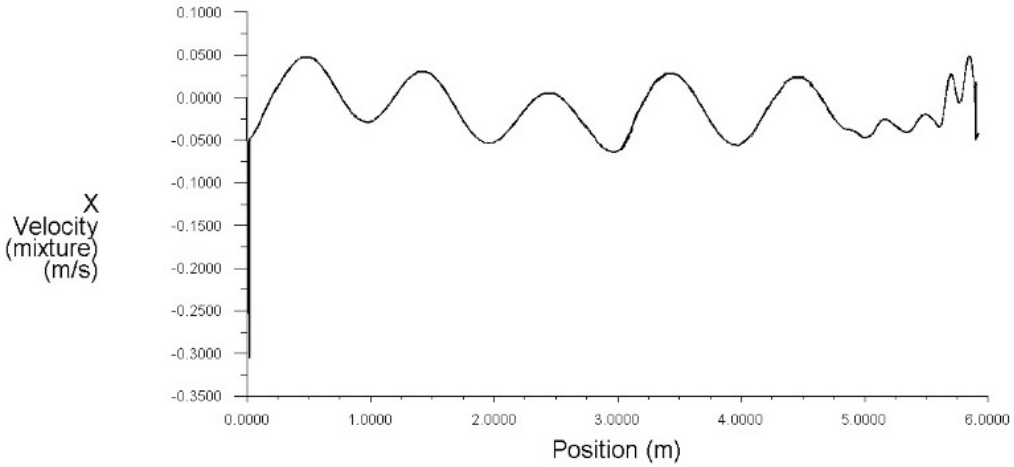

Figure 56. X-velocity vs. Position in case with damping term added.

Figure 57 and Figure 58 represent x-velocity vs. position in case without damping term added and in Case 5 with damping term added, respectively. The time selected is after the wave the backflow. In both cases, the simulations are carried out with the different parameters, wave height 0.14m, wave period 1.5s, water depth 0.5m, and wavelength 2.8m.

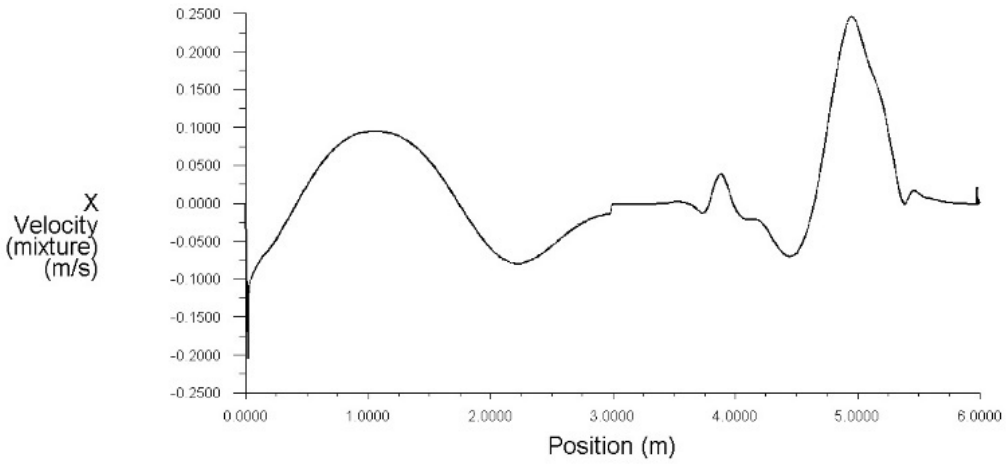

Figure 57. X-velocity vs. Position in case without damping term added.

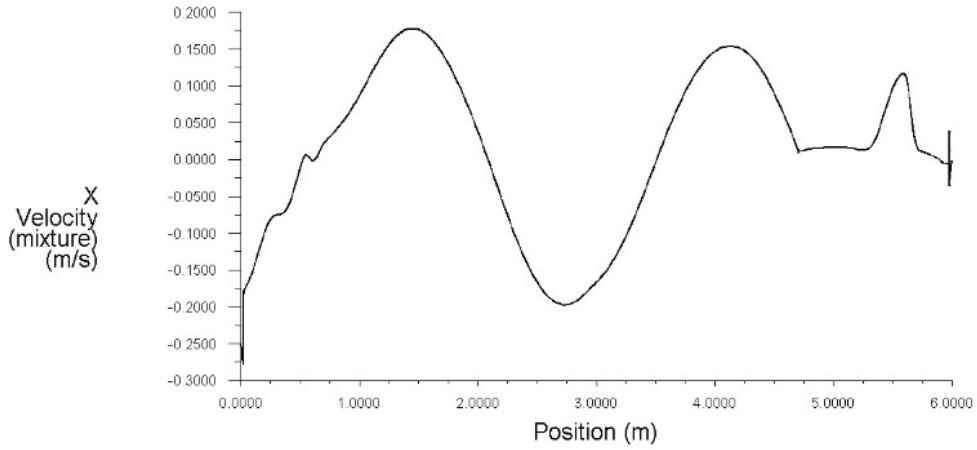

Figure 58. X-velocity vs. Position in Case 5 with damping term added.

It can be observed that the x-velocity was affected by the backflow at the end of the wave tank. By added damping term, the x-velocity has a big difference with the one without adding damping term. On the other hand, to achieve a better simulation of wave propagation, avoiding the reflection of the wave, damping term added in the momentum equation would contribute a reasonable result.

Figure 59 shows the comparison within case with damping term, case without damping term, and the analytical results at position x=0.255m, and x=0.765m. It can be detected that the backflow phenomena have not the impact on the beginning of the tank since the numerical results have a great agreement with the analytical result.

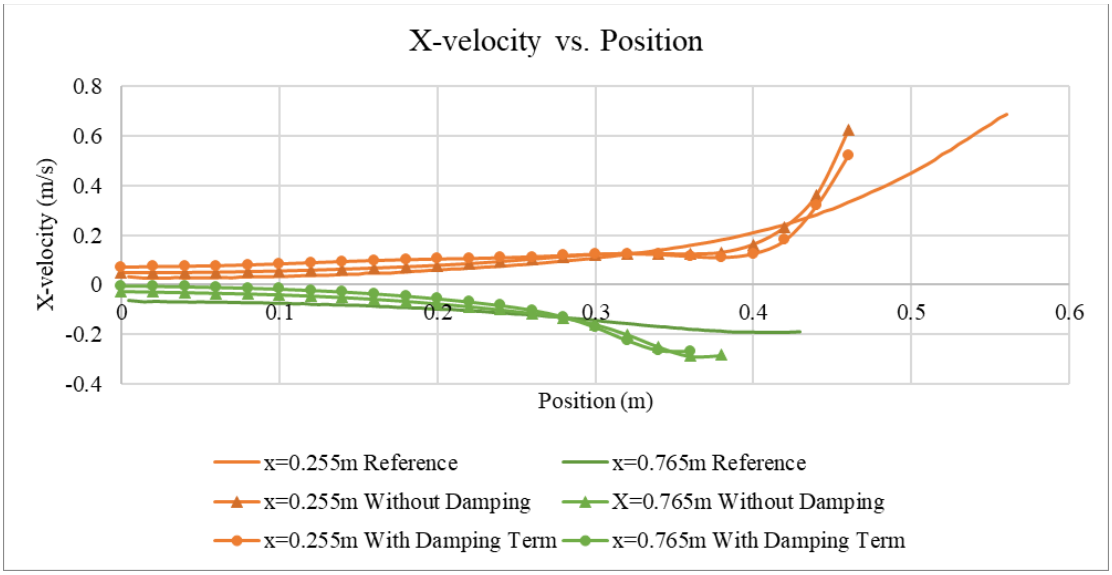

Figure 59. X-velocity at different positions.

Velocity in x direction and in z direction at position x=5.1m vs. Z-coordinate, where is at the end of the tank, is shown in Figure 60 and Figure 61. It can be noticed that the wave reflection has the influence on velocity of the wave generated.

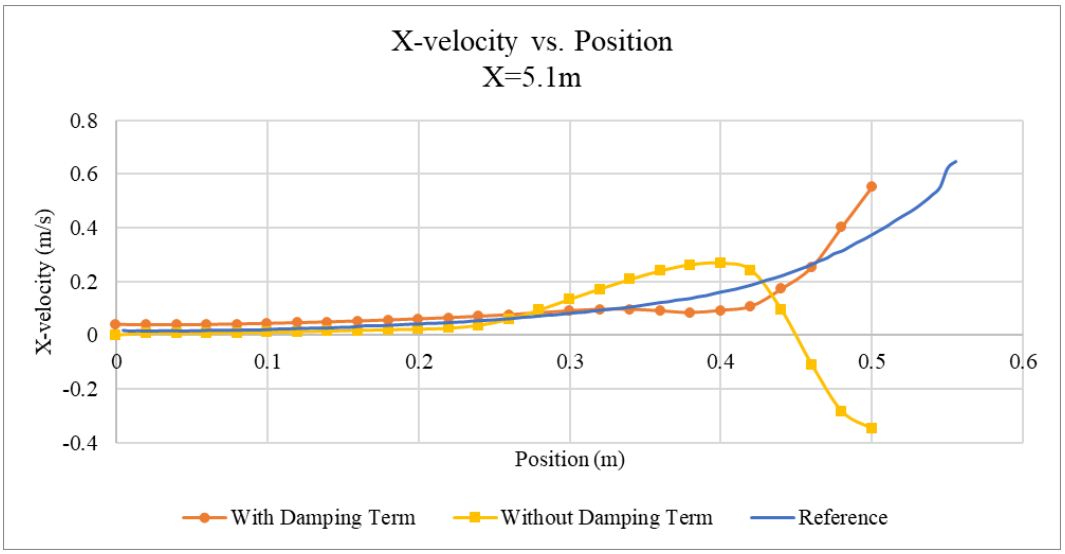

Figure 60. X-velocity at positions x=5.1m.

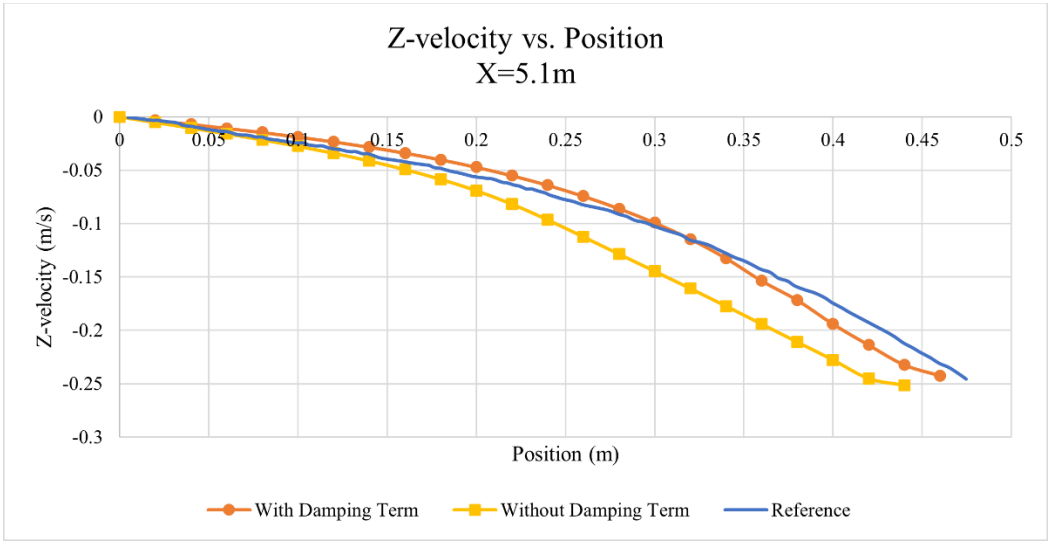

Figure 61. Z-velocity at positions x=5.1m.

Table 11 and Table 12 show the percentage error of velocity in x and in z direction at position X=5.1m between the cases with and without damping term added. It can be concluded

that there is large error of velocity in z direction in the case without damping term added due to the wave reflection.

Table 11. Error of x-velocity in wave reflection study.

X-velocity (m/s) / Position (m)	Error (%)	
	Without Damping Term	With Damping Term
Z=0.30	-35.5	0.1
Z=0.35	-48.1	1.6
Z=0.45	139.5	-24.8

Table 12. Error of z-velocity in wave reflection study.

Z-velocity (m/s) / Position (m)	Error (%)	
	Without Damping Term	With Damping Term
Z=0.25	26.5	-8.6
Z=0.30	38.1	-2.9
Z=0.35	32.1	17.9

3.6.2 X-velocity vs. Time

To further study how backflow would affect the x-velocity of the wave generated, at a function of time, different planes at different locations in fluid zone were created. Figure 62 shows different locations at z=0.5m, where at the air-water interface.

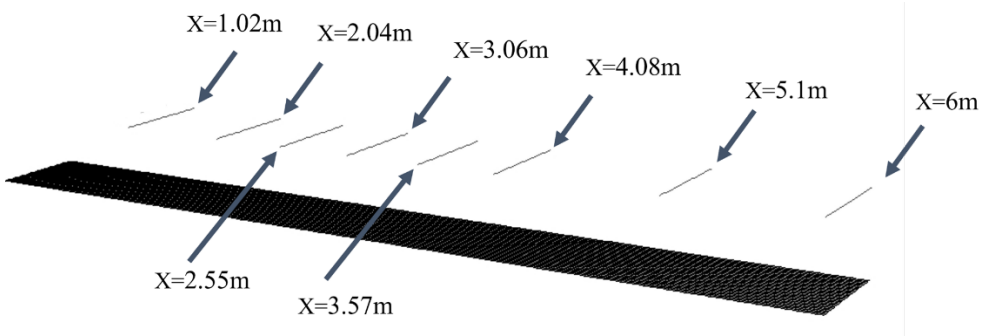

Figure 62. Different locations at z=0.5m.

Figure 63 shows the x-velocity vs. time at location x=1.02m in case with damping term added and in case without damping term added. In Figure 64, it shows the x-velocity vs. time at location x=2.04m. It can be observed that x-velocity in case without damping term added was larger than the one with damping term.

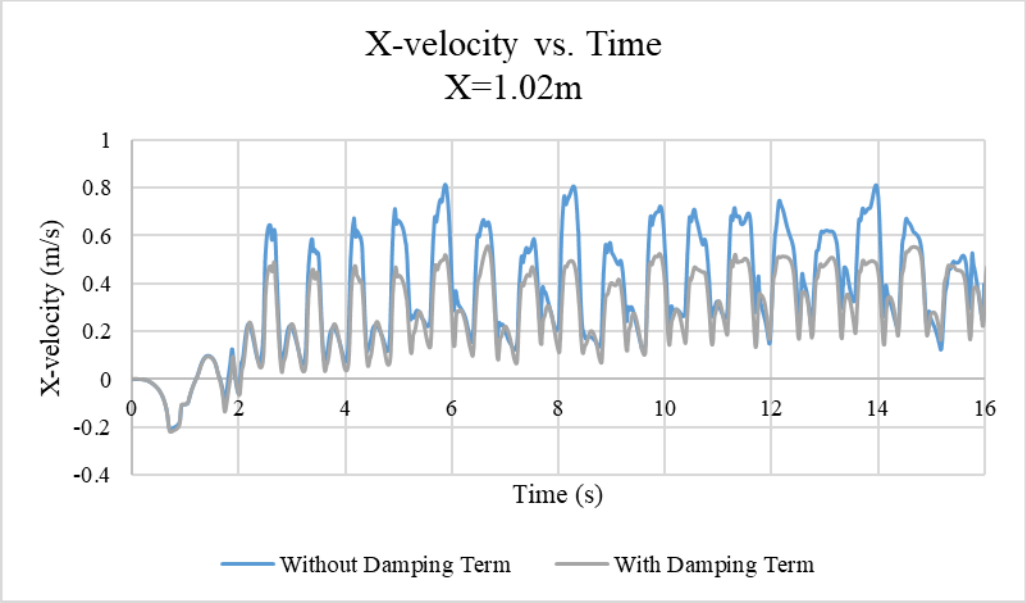

Figure 63. X-velocity vs. Time at position x=1.02m.

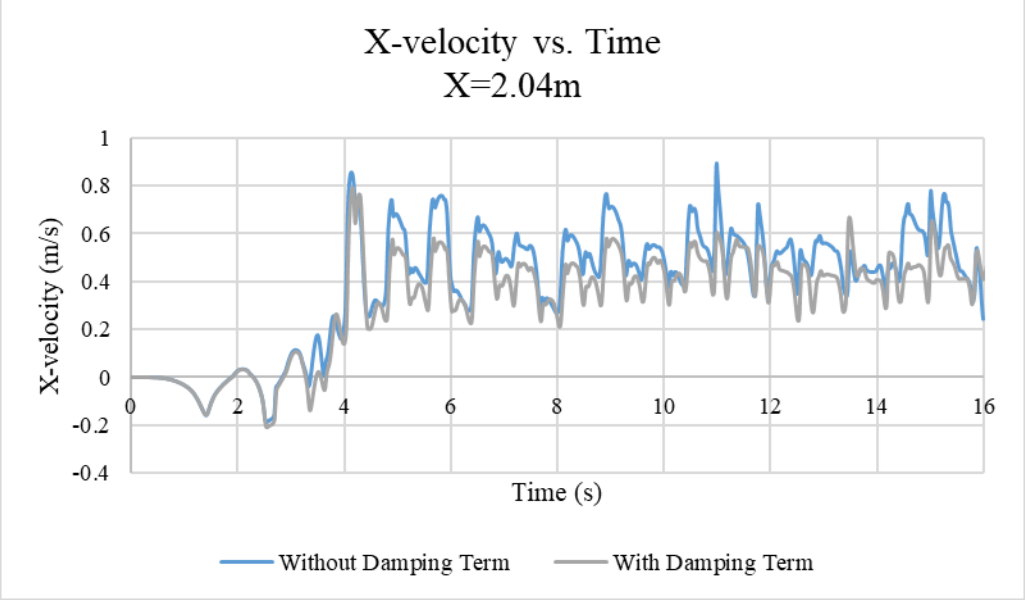

Figure 64. X-velocity vs. Time at position x=2.04m.

In Figure 65, the x-velocity in case without damping term is larger than the one in case with damping term after 4s at position x=2.55m.

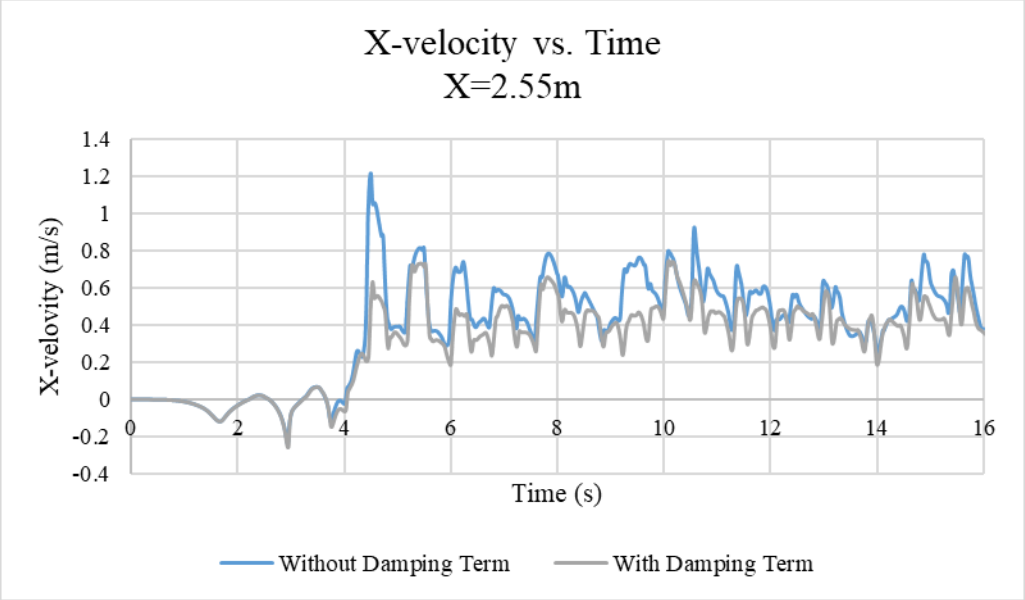

Figure 65. X-velocity vs. Time at position x= 2.55m.

Figure 66 shows the velocity in x direction in case with damping term and case without damping term. It can be observed that when time equals to 5s, x-velocity in case without damping term is much larger than the one in case with damping term. It can be concluded that with the location closing to the end of the tank, the influence of backflow is more obvious.

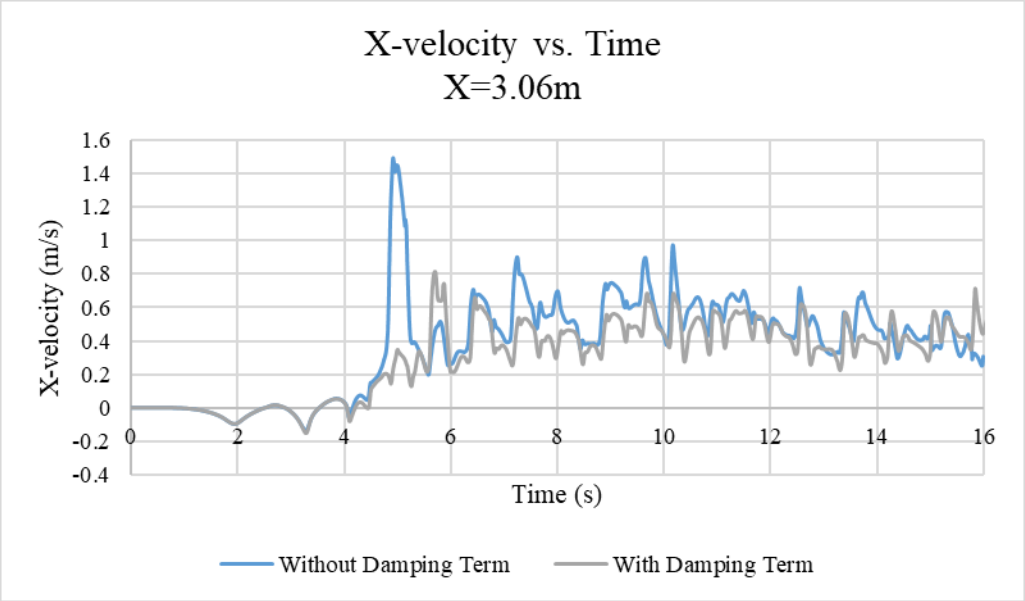

Figure 66. X-velocity vs. Time at position x= 3.06m.

In Figure 67, after 14s, the x-velocity has a huge difference between two cases, which means with the location approaching the end of the tank, backflow has a greater impact on x-velocity.

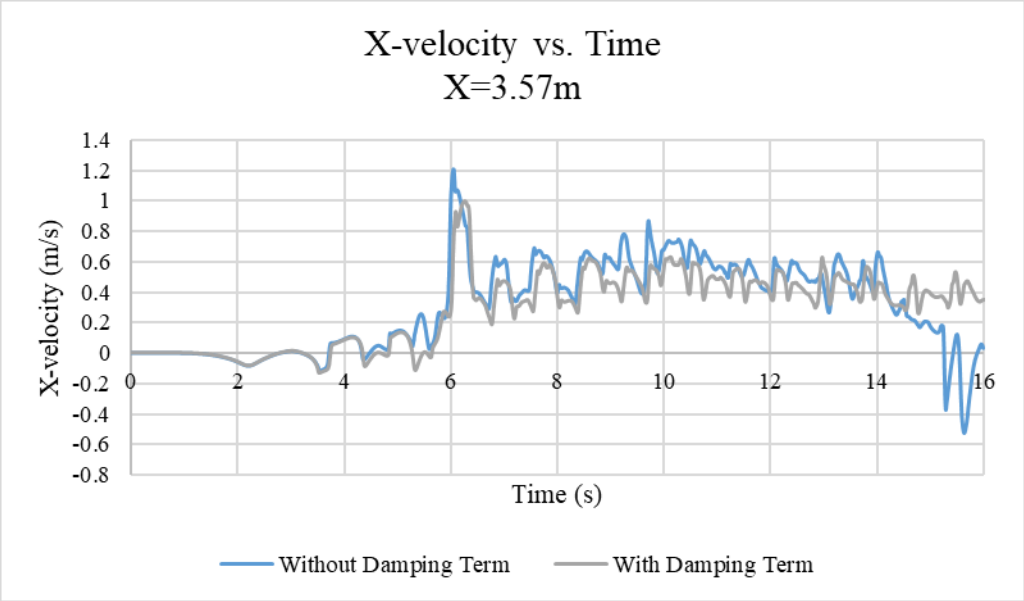

Figure 67. X-velocity vs. Time at position x= 3.57m.

X-velocity vs. time at position x=4.08m is sown in Figure 68. It can be noticed that when time equals to 6.5s, there is a sudden surge on x-velocity dur to backflow. After 13s, wave reflection has a great impact on the velocity in x direction.

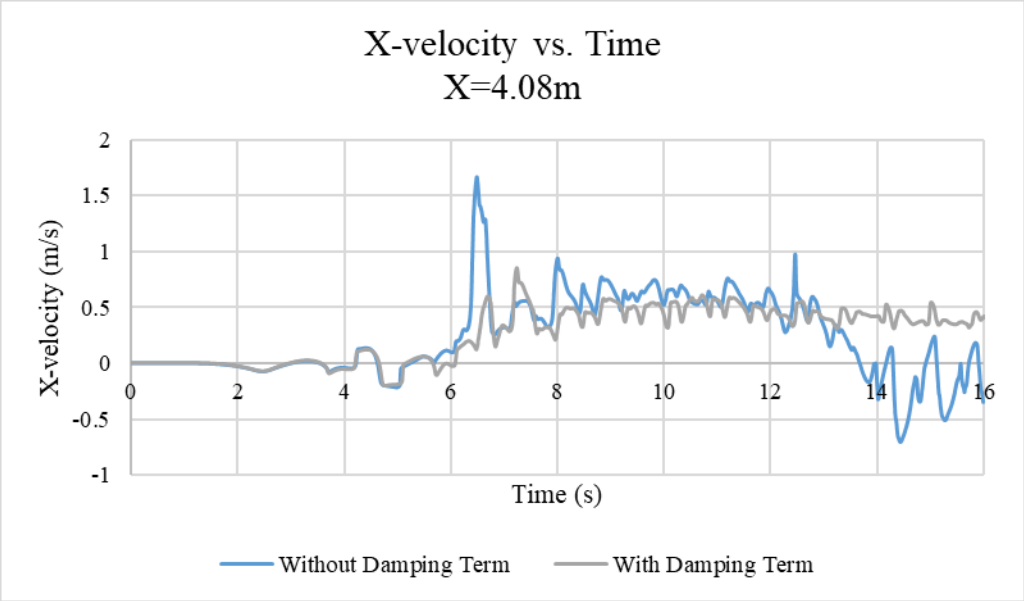

Figure 68. X-velocity vs. Time at position x= 4.08m.

Figure 69 shows the velocity in x direction at a function of time at position x=6m, where at the end of the tank. It can be seen that after 8s, the wave has reached the end of the tank, in other words, the backflow is created.

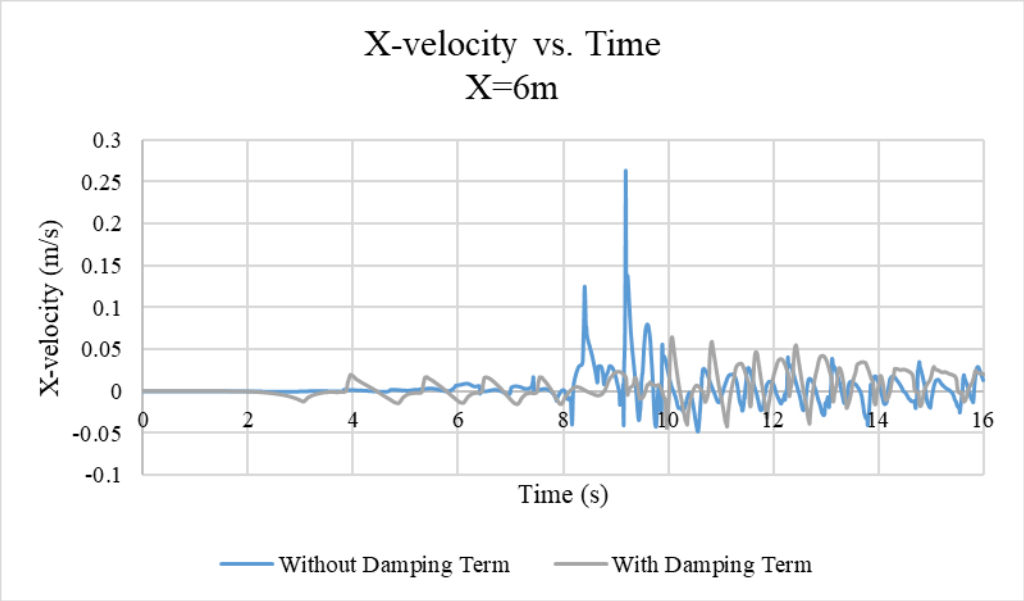

Figure 69. X-velocity vs. Time at position x= 6m.

3.6.3 Z-velocity vs. Time

Equation 16 and Equation 17, which are the velocity component in x and z direction, were applied to the inlet velocity via User Defined Function (UDF). After study the backflow impact on velocity in x direction, further study on influence on velocity in z direction is carried out. Figure 70, Figure 71, and Figure 72 show a great agreement between cases with and without damping term added for velocity in z direction at position x=1.02m, x=2.04m and x=2.55m. As a result of the location is at the beginning of the tank, there almost no effect on velocity in z direction due to the backflow.

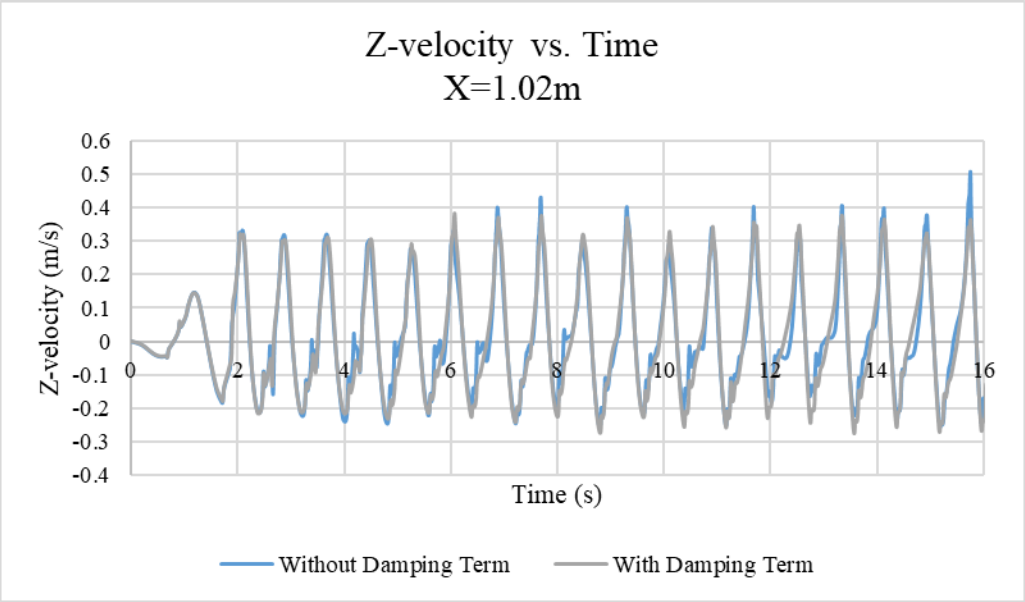

Figure 70. Z-velocity vs. Time at position x= 1.02m.

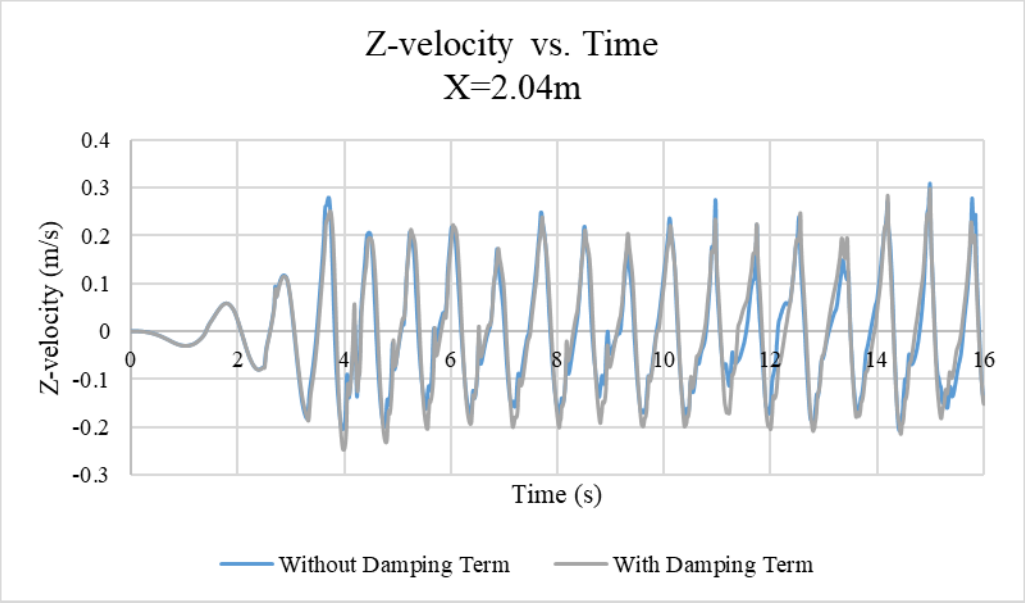

Figure 71. Z-velocity vs. Time at position x= 2.04m.

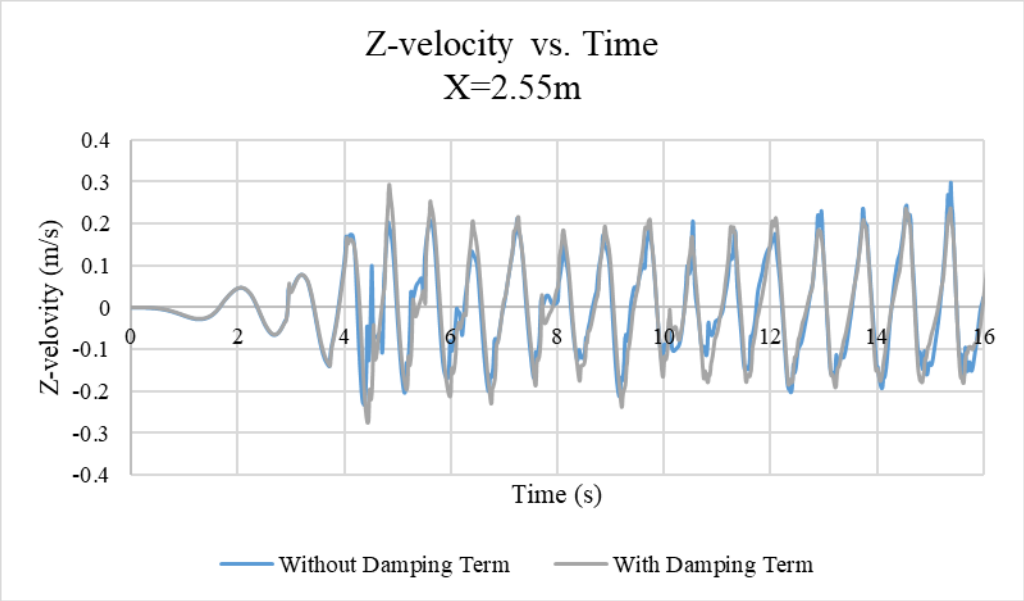

Figure 72. Z-velocity vs. Time at position x= 2.55m.

In Figure 73, Figure 74, and Figure 75, it can be observed that there have impact on velocity in z direction due to wave reflection during 4s to 8s at position x=3.06m, x=3.57m, and x=4.08m. As the plane created approaches the end of the tank, the effect of backflow becomes more pronounced. It can be seen in Figure 74 and Figure 75 that the velocity in z direction in case with backflow phenomena is obviously impacted by the reflected wave after 14s.

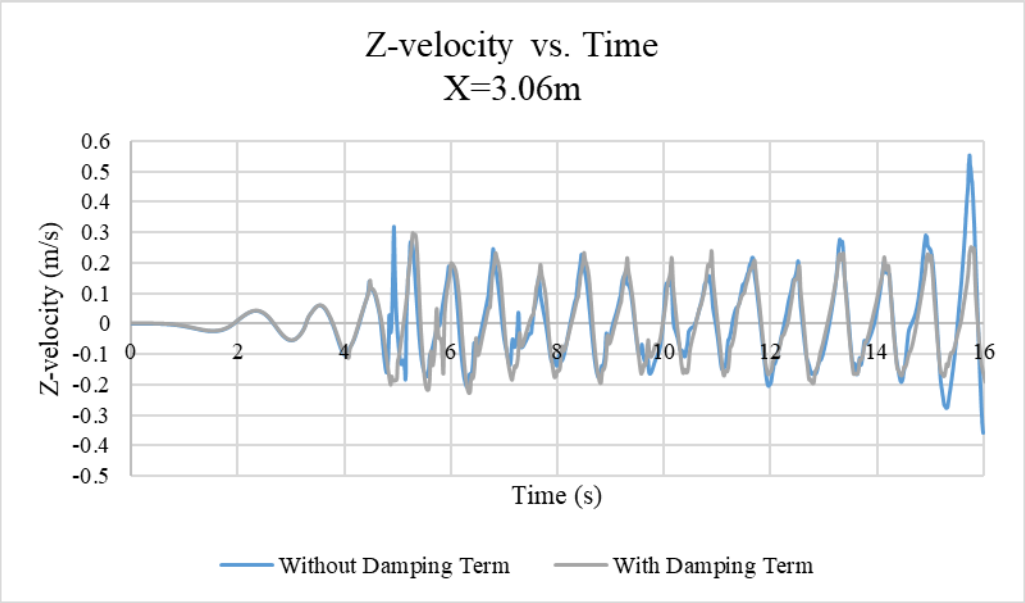

Figure 73. Z-velocity vs. Time at position x= 3.06m.

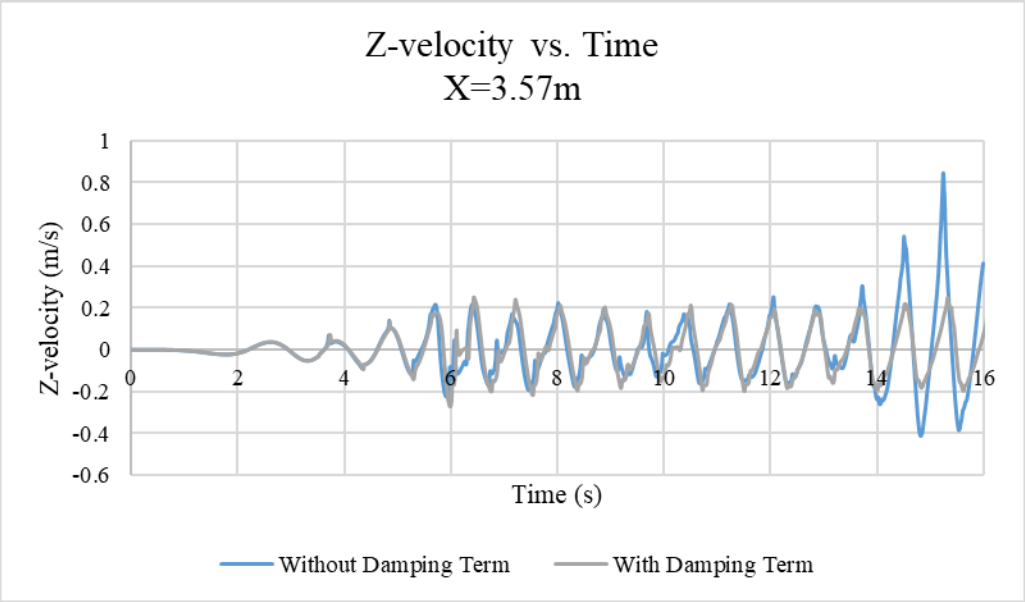

Figure 74. Z-velocity vs. Time at position x= 3.57m.

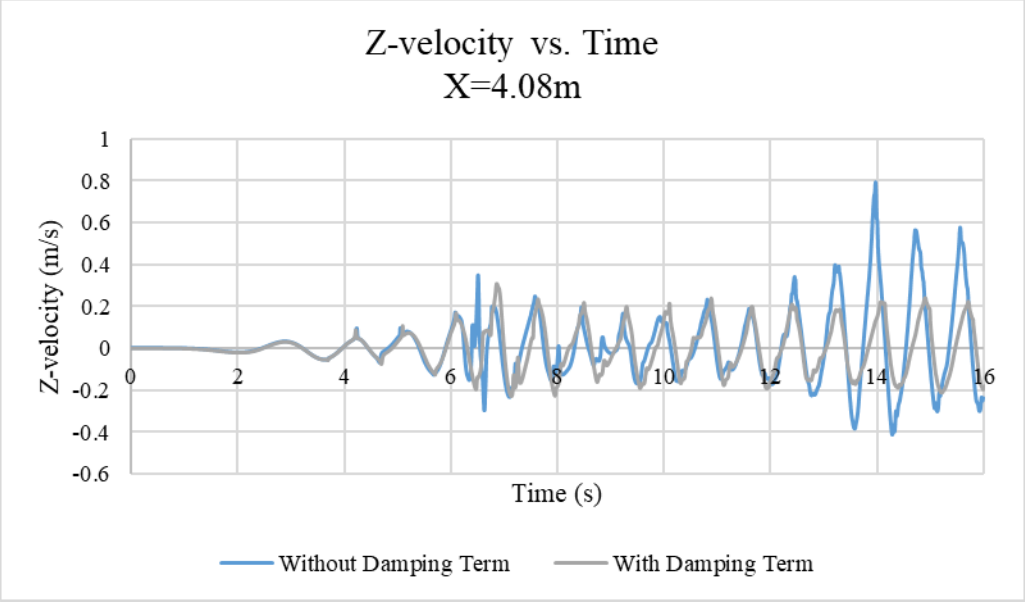

Figure 75. Z-velocity vs. Time at position x= 4.08m.

At position x=5.1 and x=6m, where at the end of the tank, velocity change in z direction at a function of time was shown in Figure 76 and Figure 77. It is clear that after 8s, the reflection of the wave occurred, which leads to the influence on z-velocity.

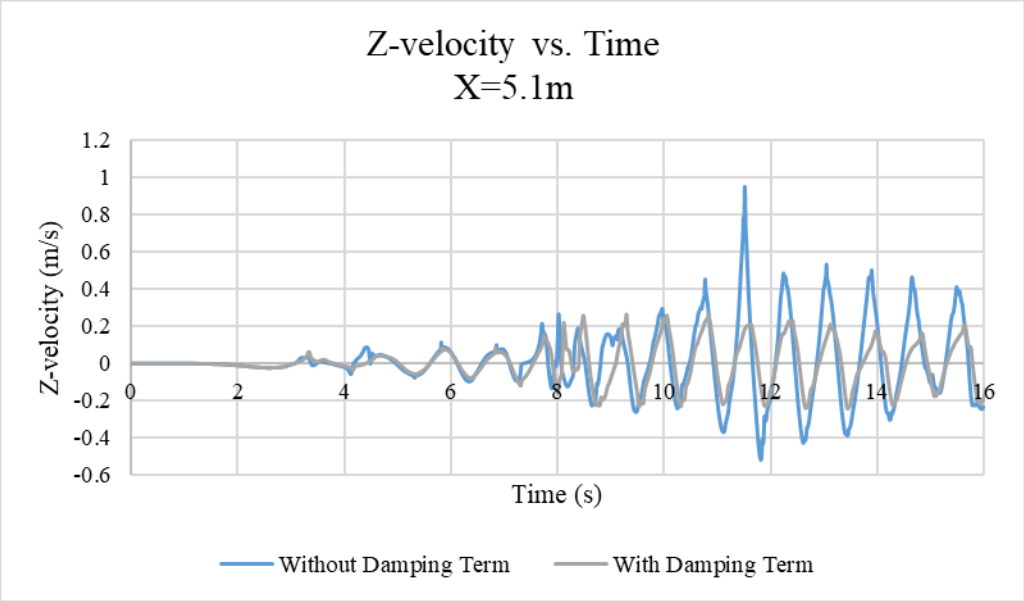

Figure 76. Z-velocity vs. Time at position x= 5.1m.

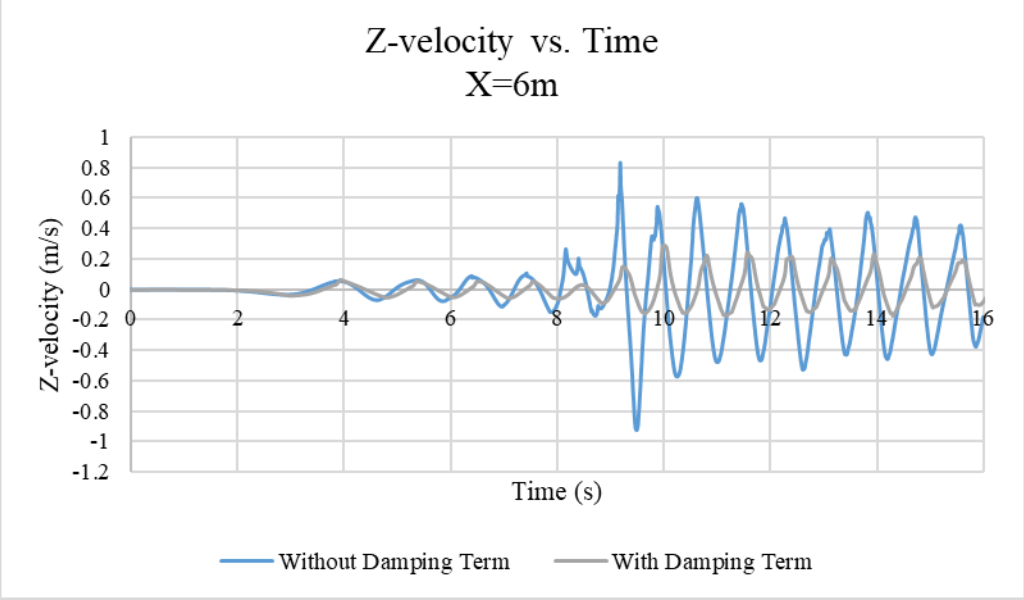

Figure 77. Z-velocity vs. Time at position x= 6m.

4. CONCLUSION

In this thesis, all the simulations are analyzed under intermediate water wave condition. Since the speed of intermediate water wave depends on wave period, wavelength and depth, to have a better study on the impact of wave period and wavelength to wave velocity, the depth remains the same in this thesis. From the numerical studies, it can be concluded that increasing in wavelength, wave velocity will increase. However, if both the wavelength and the period are increased, the combined effect of the increase in velocity will be reduced.

In mesh independence study, a coarse grid is not able to capture all the flow features and a finer mesh can give a result of a little better accuracy than required but at the expense of computational power and time. In other words, use the medium mesh is more reasonable to capture all the essential flow features, their gradients, and so forth. Consequently, the reason for performing a mesh independence study can help to have a valid result during the simulations.

After analyzing the results obtained in the simulation, the computational modeling method based on VOF model is applicable and acceptable. Compared with the numerical results, the generated wave using numerical model simulation has the desired results. As a consequence, it is possible to validate the numerical simulation technique for regular wave production by comparing the results of the numerical method to the results of numerical simulations from previous numerical studies. The Function Methodology and Mobile Methodology are able to reproduce sufficiently the connection between the liquid phase and the gas phase. The only characteristic that differs between the two methodologies of generating waves is the computational processing time, while the Function Methodology is better, which takes less time than the Mobile Methodology. The wave velocity is related to the wavelength and the wave's frequency and period. It can easily be discovered that the velocity of the connection between water and air is the biggest, and the velocity decreases to the sides of the tank.

Without adding the damping term in the momentum equation in User Define Function, the reflected wave at the end of the wave tank interferes with the generated wave, which lead to the influence of the results of the velocity along the x direction and z direction. It is essential to implement the damping term to avoid the backflow to make the simulation results more reasonable since in real ocean condition there hasn't the backflow phenomena. The coefficients in the

damping functions need to be modified to the parameters of the waves in order to obtain the reliable wave damping.

In future work, the different water depth and wave steepness will be examined. To simulation real ocean wave, other type of water wave, such as deep water wave and shallow water wave will be analyzed. To analyze the offshore wave energy, as well as wind energy, an offshore floating wind turbine will be added in the fluid domain.

REFERENCES

[1] U.S. Energy Information Administration https://www.eia.gov/energyexplained/us-energy-facts/

[2] J. C. Park, M. H. Kim, H, Miyata, H. H. Chun. Fully nonlinear numerical wave tank (NWT) simulations and wave run-up prediction around 3-D structures. *Ocean Engineering.* 2003, Volume 30. Page 1969-1996.

[3] H. W. Wang, C. J. Huang, J. Wu. Simulation of a 3D Numerical Viscous Wave Tank. *Journal of Engineering Mechanics.* 2006, Volume 133, Pages 761-772.

[4] M. Zabihi, S. Mazaheri, A. R. Mazyak. Wave Generation in a Numerical Wave Tank. *The 17th Marine Industry Conference.* December 22-25, 2015.

[5] M. N. Gomes, C. R. Olinto, L. A. O. Rocha, J. A. Souza, L. A. Isoldi. Computational Modeling of a Regular Wave Tank. *Proceedings of the 2009 3rd Southern Conference on Computational Modeling*. November 2009, Pages 60–65.

[6] A. Kamath, H. Bihs, M. A. Chella, O. A. Arntsen. CFD Simulations of Wave Propagation and Shoaling over a Submerged Bar. *Aquatic Procedia.* 2015, Volume 4, Pages 308-316.

[7] P. Schmitt, C. Windt, J. Davidson, J. V. Ringwood, T. Whittaker. The Efficient Application of an Impulse Source Wavemaker to CFD Simulations. *Journal of Marine Science and Engineering.* 2019, Volume 3, Page 71.

[8] W. Wang, A. Kamath, T. Martin, C. Pákozdi, H. Bihs. A Comparison of Different Wave Modelling Techniques in An Open-Source Hydrodynamic Framework. *Journal of Marine Science and Engineering.* 2020, Volume 8, Page 526.

[9] B. Yang, J. Deng, K. Liu, F. Ye. Theory Analysis and CFD Simulation of the Pressure Wave Generator. *Journal of Chemical Engineering Transactions*. 2017, Volume 61, Pages 481-487.

[10] Z. Li, G. Deng, P. Queutey, B. Bouscasse, G. Ducrozet, L. Gentaz, D. L. Touzé, P. Ferrant. Comparison of wave modeling methods in CFD solvers for ocean engineering applications. *Ocean Engineering*. 2019, Volume 188, Page 106237.

[11] Y. M. Choi, Y. J. Kim, B. Bouscasse, S. Seng, L. Gentaz, P. Ferrant. Performance of different techniques of generation and absorption of free-surface waves in Computational Fluid Dynamics. *Ocean Engineering.* 2020, Volume 214, Page 107575.

[12] K. Yousefi, F. Veron. Boundary layer formulations in orthogonal curvilinear coordinates for flow over wind-generated surface waves. *Journal of Fluid Mechanics*. 2020, Volume 888.

[13] N. T. Husain, T. Hara, M. P. Buckley, K. Yousefi, F. Veron, P. P. Sullivan. Boundary Layer Turbulence over Surface Waves in a Strongly Forced Condition: LES and Observation. *Journal of Physical Oceanography*. Volume 49, Pages 1997-2015.

[14] M. E. McCormick. *Ocean engineering wave mechanics*. John Wiley & Sons, USA, New York. 1976.

[15] R. G. Dean, R. A. Dalrymple. Water wave mechanics for engineers and scientists. *World scientific*. Singapore. 1991, Volume 2.

[16] M. Horko. CFD Optimization of an Oscillating Water Column Energy converter, Thesis of Master of Engineering Science, School of Mechanical Engineering, The University of Western, Australia. 2007.

[17] E. Liu. Application of Numerical Wave Tank to OWC air chamber for wave energy conversion. *Proceedings of the Eighteenth International Offshore and Polar Engineering Conference*. Vancouver, Canada. 2008.

[18] ANSYS FLUENT 12.0/12.1 Documentation. *Volume of Fluid (VOF) Model Theory*. Chapter 16.3.
https://www.afs.enea.it/project/neptunius/docs/fluent/html/th/node297.htm

[19] ANSYS FLUENT 12.0/12.1 Documentation. *DEFINE_PROPERTY UDFs*. Chapter 2.3.16.
https://www.afs.enea.it/project/neptunius/docs/fluent/html/udf/node46.htm

[20] Simulation of Wave Generation in a Tank. *Fluent Tutorial 10*.
https://willem.engen.nl/uni/fluent/documents/external/wave.pdf